MICRO SCALE HYDRODYNAMIC CAVITATION FOR THROMBOLYSIS: A NOVEL CLOT-ON-A-CHIP PLATFORM

by
BEYZANUR ÖZOGUL

Submitted to the Graduate School of Engineering and Natural Sciences
in partial fulfilment of
the requirements for the degree of Master of Science

Sabancı University
December 2023

ABSTRACT

MICRO SCALE HYDRODYNAMIC CAVITATION FOR THROMBOLYSIS: A NOVEL CLOT-ON-A-CHIP PLATFORM

BEYZANUR ÖZOGUL

Molecular Biology, Genetics and Bioengineering, MSc Thesis, December 2023

Thesis Advisor: Asst. Prof. Morteza Ghorbani

Thesis Co-advisor: Prof. Ali Koşar

Keywords: Thrombosis, Thrombolysis, Lab-on-a-Chip, Microfluidics, Microfluidic applications, Hydrodynamic cavitation

Hydrodynamic cavitation (HC) is a physical phenomenon, characterized by the formation, growth, and collapse of bubbles within a moving liquid due to pressure fluctuations. These collapsing bubbles provide high energy. Even though macro scale HC can cause undesired destructive effects, the collapse of micro scale HC bubbles releases highly localized and controllable energy, making it a promising tool for biomedical applications. Thrombosis related diseases such as deep vein thrombosis and pulmonary embolism pose a significant global health issue. Current treatments techniques are limited and might cause serious adverse effects. In this regard, this study presents an investigation of a novel platform called Clot-on-a-Chip related to micro scale HC induced thrombolysis. By utilizing microfluidic system approach, the CoC platform facilitates controlled HC bubble formation and collapse within a confined environment and targeted HC bubbles in a microfluidic device directly at thrombus. *In vitro* experiments demonstrate the success of the platform in generating HC and effectively inducing thrombolysis. These findings suggest the CoC platform has a considerable promise as a novel treatment approach for undesired blood clot formation.

ÖZET

Tromboliz için Mikro Ölçekli Hidrodinamik Kavitasyon: Yenilikçi Bir Pıhtı Üzerinde Çip Platformu

BEYZANUR ÖZOGUL

Moleküler Biyoloji, Genetik ve Biyomühendislik Yüksek Lisans Tezi, Aralık 2023

Tez Danışmanı: Asst. Prof. Morteza Ghorbani
Tez Eş Danışmanı: Prof. Dr. Ali Koşar

Anahtar Kelimeler: Tromboz, Tromboliz, Çip Üzerinde Laboratuvar, Mikroakışkanlar, Mikroakışkan uygulamalar, Hidrodinamik kavitasyon

Hidrodinamik kavitasyon (HC), basınçtaki değişimler nedeniyle hareketli bir sıvı içinde kabarcıkların oluşması, büyümesi ve patlaması ile karakterize edilen fiziksel bir olgudur. Bu çöken kabarcıklar yüksek enerji açığa çıkarır. Makro ölçekli HC, istenmeyen yıkıcı etkilere neden olsa da, mikro ölçekli HC kabarcıklarının çökmesi, oldukça lokalize ve kontrol edilebilir enerji açığa çıkarır ve bu da onu biyomedikal uygulamalar için umut verici bir araç haline getirir. Derin ven trombozu ve pulmoner emboli gibi tromboza bağlı hastalıklar önemli bir küresel yük oluşturmaktadır. Mevcut tedavi teknikleri sınırlıdır ve ciddi olumsuz etkilere neden olabilir. Bu bağlamda, bu çalışma, mikro ölçekli HC'nin neden olduğu tromboliz için Çip-üstü-pıhtı (CoC) adı verilen yeni bir platformun araştırmasını ve testini sunmaktadır. CoC platformu, mikroakışkan cihaz konseptini kullanarak kontrollü HC kabarcığı oluşumunu ve kapalı bir ortamda çökmesini kolaylaştırarak bu HC kabarcıklarını doğrudan trombusta hedef almaktadır. Gerçekleştirlen *in vitro* deneyler, platformun HC üretmedeki ve trombolizi etkili bir şekilde indüklemedeki başarısını göstermektedir. Bu bulgular, CoC platformunun istenmeyen kan pıhtısı oluşumuna karşı yeni bir tedavi olarak önemli umut vaat ettiğini göstermektedir.

ACKNOWLEDGEMENTS

Firstly, I must express my sincere appreciation to my advisors, Prof Dr. Ali Kosar and Asst. Prof. Dr. Morteza Ghorbani, whose expertise and understanding added considerably to my graduate experience. I am extremely thankful for the guidance, encouragement, and insightful critiques of my research work.

I wish to thank the members of my thesis committee, Assoc. Prof. Dr. Özlem Kutlu, Dr. Sibel Çetinel, and Dr. Tuğrul Elverdi, for their time and thoughtful feedback.

Special thanks are due to Ünal Akar and Rabia Mercimek, whose support and collaborative efforts both in and outside of the laboratory made this research possible.

My heartfelt appreciation goes to my dear friends, especially Erçil Toyran and Farzad Rokhsar Talabazar, for the stimulating discussions, for the sleepless nights we were working together, and for all the fun we have had in the last year.

Furthermore, my deepest gratitude is reserved for Ali Eray. Thank you for always being there for me.

Last but certainly not least, I must express my very profound gratitude to my family for providing me with unfailing support and continuous encouragement throughout my years of study and through the process of researching and writing this thesis. This accomplishment would not have been possible without them.

Additionally, I would like to acknowledge Scientific and Technological Research Council of Turkey (TUBITAK), for supporting this project with Grant No. 221M421.

TABLE OF CONTENTS

LIST OF TABLES

LIST OF FIGURES

LIST OF ABBREVIATIONS

FXIIIa: Factor XIIIa

DVT: Deep vein thrombosis

PE: Pulmonary embolism

VTE: Venous thromboembolism

CDT: Catheter-directed thrombolysis

UACDT: Ultrasound-assisted catheter-directed thrombolysis

HIFU: High-intensity focused ultrasound

AC: Acoustic cavitation

HC: Hydrodynamic cavitation

CoC: Clot-on-a-chip

PDMS: polydimethylsiloxane

DRIE: Deep reactive ion etching

SEM: Scanning electron microscopy

PBS: Phosphate-buffered saline

PLA: Polylactic acid

ANOVA: One-way analysis of variance

1. INTRODUCTION

1.1. Blood Coagulation

The blood coagulation process is a desired event if there is vascular tissue injury. However, if it occurs in a healthy blood artery, it might lead to some serious complications and even fatality. The blood clot is mainly made up of two components cross-linked fibrin proteins and platelets. Fibrinogen is a soluble, large glycoprotein (340 kDa) and consists of two identical subsets. These subsets comprise three polypeptides namely are Aα-, Bß-, and γ- chains cantilevered by a total of 29 disulfide bonds (Bridge et al., 2014). The E-region, which is the center section of the molecule and contains the thrombin cleavage sites, is where all six chains come together (Pechik et al., 2006).

The N-terminal fibrinopeptides A and B are produced by the thrombin cleavage of the Aα-, and Bß- chains, respectively (Weisel & Litvinov, n.d.). This is the beginning of the formation of fibrin fibers by the conversion of fibrinogen to disulfide-linked trinodular fibrin monomers. The 3D mesh-like clot structure is created when fibrin strands become intertwined. Later, factor XIIIa (FXIIIa) stabilizes fibrin clot via intermolecular covalent γ-glutamyl-ε-lysyl cross-links between residues in the Aα and γ chains of fibrin monomers (Versteeg et al., 2013). This provides clots to be more stable to enzymatic cleavage and shear forces. Platelets, also called thrombocytes, are the smallest component of blood and are made from the quite bulky bone marrow cells called megakaryocytes (Patel et al., 2005). They have a major role in hemostasis and thrombosis. Platelets become activated when tissue is injured and they adhere to one another, and aggregate. These actions cause coagulation factors and other mediators to be stimulated, which results in hemostasis. Hemostasis is a procedure to stop bleeding by retaining the blood within the damaged vessel walls. The intricate interaction among platelets, plasma

coagulation cascades, fibrinolytic proteins, blood vessels, and cytokine mediators is essential for the complicated process of hemostasis (Periayah et al., 2017). It can be examined under three different phases which include blood clotting, platelet activation, and vascular repair (Yau et al., 2015a). First, damage to the vascular tissue makes platelets activate and stick together. The second stage of hemostasis, platelet aggregation, can trigger a cascade of coagulations that results in the development of a clot consisting of aggregated cells with fibrin strand production. Finally, the location of coagulation is on the surface of activated platelets, and fibrinolysis with clot solution improves wound healing (Opneja et al., n.d.).

1.2. Thrombosis

Thrombosis is the pathological formation of blood clots within arteries or veins that restrict natural blood flow due to severely active hemostasis or improperly activated platelets and might cause serious diseases. Thrombus can be named according to the type of vessels where it occurs. It is called arterial thrombus when it occurs in arterials, and it is called venous thrombus when it occurs in veins. Accordingly, the structure of the thrombus differs between venous and arterial. Arterial thrombi mainly consist of an aggregation of platelets that gives a white-clot appearance, and it occurs when an atherosclerotic plaque ruptures, and monocytes, lymphocytes, and smooth muscle cells congregate in the artery wall as a result of endothelium damage (Yau et al., 2015b). Treatment for this kind of clot is urgent. Venous thrombi are known as red clots because they are mostly made of red blood cells and fibrin. It could happen because of altered blood composition that promotes thrombosis, altered blood flow—either increased or decreased—or altered vessel walls (Lippi et al., 2011). Even though these blood clots may form more gradually over time, they might still be fatal. Venous thrombi often develop around an uninjured endothelium wall in low-shear flow regions. On the other hand, an embolus is a mass that moves through the circulation and can cause blockage of blood when it reaches a vessel that is too small to let it pass. An embolism or embolic event occurs when an embolus occludes a blood vessel. Moreover, plasma levels of fibrinogen quickly rise in inflammatory situations. In reaction to pro-inflammatory substances like interleukin-6 and other cytokines, fibrinogen expression is sharply up-regulated, and

enhanced gene transcription results in larger amounts of circulating fibrinogen (Bridge et al., 2014). Numerous thrombotic disorders, including pulmonary embolism, peripheral vascular disease (Bartlett et al., 2009) stroke (Tanne et al., 2001), and cardiovascular disease (CVD) (Scarabin et al., 2003) have been linked to elevated plasma levels of fibrinogen.

1.2.1. Thrombotic Disorders

Pulmonary embolism (PE) and deep vein thrombosis (DVT) are two types of venous thromboembolism (VTE), which affects 1 to 2 in 1,000 people yearly and is the third most prevalent cause of vascular mortality after myocardial infarction and stroke (Fleck et al., 2017). In the peripheral circulation, deep vein thrombosis occurs most frequently in the leg, groin, or arm deep veins. When the clot moves through the circulation and lodges in the pulmonary trunk, the major pulmonary artery, or the segmental or sub-segmental branches, it might result in the most serious condition, pulmonary embolism. Rudolf Virchow identified the primary pathogenic causes of DVT and PE in 1859 (López et al., 2004). Virchow concluded that (1) venous stasis, (2) alterations in the vascular wall, and (3) hypercoagulability were the main causes of the formation of venous thrombosis based on finely thorough and perceptive pathologic observations (Bagot & Arya, 2008). This triad is still valid since each of these three processes is influenced by all prothrombotic stimuli, whether they are systemic or molecular. Nevertheless, there are many other clinical variables that are linked to VTE such as obesity, chronic illness, pregnancy, surgery or trauma, immobility, varicose veins, and both genetic and environmental factors (Pastori et al., 2023) .

Ischemic stroke is another serious condition that can be brought on by a blood clot forming in a blood artery in the brain or neck, or by a clot moving from another region of the body to the brain, such as the heart, thereby blocking a blood vessel in the neck or brain (Randolph, 2016). The World Health Organization estimates that 6.2 million individuals worldwide died from stroke in 2019, accounting for nearly 87% of ischemic stroke-related mortality (Owens Johnson et al., 2019).

1.2.2. Therapeutic Approaches against Venous Thrombosis

Different treatment options are being used for VTE which can be examined under two categories conventional and alternative therapeutic approaches. Any therapy, which is intended to dissolve potentially harmful blood clots in blood arteries, enhances blood flow, and reduces organ and tissue damage, is referred to as thrombolysis, sometimes known as thrombolytic therapy (Ramjan Ali et al., 2014). It is used to treat acute arterial and deep vein thrombosis as well as ischemic cerebrovascular stroke and pulmonary embolism. When a thrombolytic drug starts the process of converting the inactive proenzyme plasminogen to the active serine plasmin, it causes thrombolysis, which is biochemically the proteolysis of a fibrin network. Although thrombolysis is a biochemical process that resembles a cascade and involves several different proteins, it also heavily depends on the hemodynamic circumstances at the location of the clot. Conventional approaches mainly consist of anticoagulants, systemic thrombolysis, and catheter-directed thrombolysis.

1.2.2.1. Conventional Thrombolytic Therapeutic Approaches against Venous Thrombosis

A frequent conventional treatment for VTE is anticoagulant therapy. This treatment lowers the possibility of blood clots developing in the veins and eliminates further complications. Heparin, warfarin, and low molecular weight heparin are examples of anticoagulants that function by obstructing the development of new blood clots and assisting in preventing the growth of existing clots (Bates & Weitz, 2005). These drugs also assist in lowering the risk of PE. Both short-term and long-term treatments for VTE are possible with anticoagulant medication, which can also lower the likelihood of recurrence and avoid subsequent problems. Anticoagulant therapy can be divided into three, phases which are the acute phase, maintenance phase, and extended phase, as stated in Table 1 (Nisio, D.,2016).

Table 1. Phases of anticoagulant therapy for venous thromboembolism (Di Nisio et al., 2016).

Phases Of Anticoagulant Therapy	Description	Duration
Acute Phase (Nutescu et al., n.d.)	Treatment options consist of subcutaneous low-molecular-weight heparin or fondaparinux, intravenous unfractionated heparin, or the direct oral factor Xa inhibitors rivaroxaban and apixaban.	First 5-10 days after diagnosis
Maintenance Phase (Nutescu et al., n.d.)	Maintaining an effective anticoagulant effect, while minimizing the risk of adverse side effects.	3-6 months
Extended Phase (Yeh et al., 2014)	Ensuring the risk of clot formation is minimized and the patient is transitioned to other therapies as needed.	Beyond this period

The choice of initial anticoagulant therapy for VTE prioritizes in preventing further clot formation, even if complete resolution of the underlying cause remains a challenge. Treatment options range from intravenous unfractionated heparin to direct oral factor Xa inhibitors, with low-molecular-weight heparin and fondaparinux generally preferred for their safety and efficacy (Umerah & Momodu, 2023). Unfractionated heparin finds specific utility in thrombolysis due to its rapid reversibility with protamine and ease of monitoring. Heparin-induced thrombocytopenia necessitates immediate discontinuation and alternative parenteral anticoagulation with agents like fondaparinux, argatroban, or lepirudin (Ahmed et al., 2007). Prolonging anticoagulation therapy depends on a delicate balance between preventing recurrent VTE and the potential for life-threatening bleeding. While pharmacological therapy remains suitable for hemodynamically unstable PE patients, where the benefits outweigh bleeding risks, limitations come into play (Yamamoto, 2018). Notably, clearance of these drugs heavily relies on a functioning liver, which requires careful administration in patients with hepatic impairment. Additionally, increased risks of hemorrhage, hemorrhagic stroke, and cerebral hemorrhage are established concerns associated with anticoagulant therapy.

Another conventional therapy that has been widely used in thrombosis is thrombolytic therapy which administers the thrombolytic agensts such as recombinant tissue

plasminogen activator (rt-PA) (Zhang et al., 2023). One of two mammalian proteases that convert plasminogen into active plasmin is the serine protease tissue plasminoNR1gen activator (tPA), which results in the dissolution of fibrin clots (Vassalli et al., n.d.). The related mechanism is illustrated in Figure 1. This is the motivation for the creation of a recombinant version of tPA (rt-PA), which is the only FDA-approved medication for clinical use. This recombinant version of tPA has been modified in a variety of ways to improve its pharmacokinetics and pharmacodynamics, most notably by extending its short half-life in circulation and enhancing its fibrin specificity to avoid an undesirable fibrinolytic condition (Gravanis & Tsirka, n.d.).

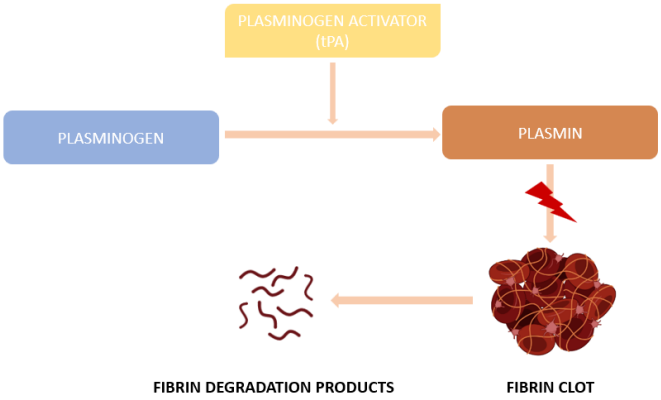

Figure 1. Illustration of dissolution of fibrin clots (fibrinolysis)

Unfortunately, the utilization of rt-PA is restricted due to possible severe adverse effects. The most frequent side effect is bleeding, and the most severe is a stroke (Jilani & Siddiqui, 2023). Other side effects observed are hypotension, nausea/vomiting, bruising, thromboembolism, muscle pain, allergic reaction, intracranial hemorrhage, arterial embolism, deep vein thrombosis, seizure, and sepsis (Jilani & Siddiqui, 2023).

Another conventional therapy used in the treatment of thrombosis-related diseases is catheter-directed thrombolysis (CDT). CDT entails percutaneously inserting a catheter into the venous system, followed by fluoroscopic guiding to the target vessel and sustained infusion of a thrombolytic drug like tPA straight into the thrombus (Fleck et al., 2017). Total thrombolytic dosage is decreased, and systemic medication exposure is limited in CDT drops. Furthermore, this treatment method lowers the risk of systemic hemorrhage while maximizing lytic agent exposure to the clot (Fleck et al., 2017). CDT has several advantages over systemic thrombolytic treatment, including enhanced drug

delivery efficiency, reduced total drug amount, and lower likelihood of post-thrombotic syndrome (Goldhaber et al., 2021). Notwithstanding its possible benefits, CDT is associated with increased risks of significant bleeding and most problems can arise due to significant bleeding. For example, a hemorrhagic stroke is one of the most prevalent and dreaded complications, with potentially disastrous consequences for the patient (Unnithan et al., 2023). Additional common consequences include pulmonary hemorrhage, pulmonary artery rupture or dissection, arrhythmias, and cardiogenic shock (Ribas et al., 2021). Table 2 summarizes the advantages and disadvantages of conventional treatments that have been used in venous thromboembolism.

Table 2. Advantages and disadvantages of conventional treatments for vascular thrombosis.

TREATMENTS	ADVANTAGES	DISADVANTAGES
Anticoagulants (Harter et al., 2015)	- Reduces the risk of developing blood clots and further complications	- Does not remove clot completely - Risk of developing post-thrombotic syndrome (PTS) - Hemorrhage
Systemic Thrombolysis (Martin et al., 2016)	- It actively breaks down clot	- Increased risk of serious bleeding complications - Can lead to stroke - Seizure - Sepsis
Catheter-Directed Thrombolysis (Fleck et al., 2017)	- Preventing valvular damage - Restores venous patency more quickly than anticoagulation - Hastening the resolution of acute symptoms.	- May cause intracranial bleeding - Rather costly

As seen in Table 2, conventional treatment methods present different disadvantages that might cause minor complications to the patient or can lead to serious side effects such as intracranial bleeding. To address the limits of pharmaceutical thrombolysis, alternative treatments have been studied.

1.2.2.2. Alternative Thrombolytic Therapeutic Approaches against Venous Thrombosis

Sonothrombolysis can be defined as the use of ultrasound energy in thrombolysis treatment with or without microbubbles (Dixon et al., 1965). This technique has been utilized since the late 1980s and the working mechanism of this technique is mainly dissolving fibrin clots by inducing stable cavitation, inertial cavitation, micro-streaming, and acoustic radiation force (Goel & Jiang, n.d.). Also, it can be used with systemic

thrombolysis such as tPA to increase the efficiency of treatment by increasing the quantity of focused cavitation, thereby eliminating blood clots while reducing clot debris (Francis et al., 1995). Ultrasound-assisted catheter-directed thrombolysis (UACDT) is a type of pharmacomechanical thrombolysis that uses a catheter to deliver ultrasound waves into blood clots (Engelberger et al., n.d.) On the other hand, microbubble-mediated intravascular sonothrombolysis is a blood clot therapy that uses microbubbles and ultrasound waves (Lu et al., 2016). Microbubbles, which are small gas-filled bubbles, are injected into the circulation together with clot-dissolving medicine as part of the treatment. After the microbubbles have passed through the blood vessels, high-frequency ultrasound waves are directed at the site of the obstruction. When subjected to ultrasound, microbubbles undergo volumetric oscillations, which cause the surrounding fluid to flow, a phenomenon known as cavitation microstreaming. This method enhances the effect of clot-dissolving drug, allowing it to dissolve the clot more efficiently. There have been many studies conducted to develop a treatment for thrombosis using sonothrombolysis with different approaches. For example, (Suo et al., 2015) investigated in using multi-frequency acoustic waves at MHz range near 1.5 MHz as high-intensity focused ultrasound (HIFU) excitations to reduce power and treatment time. In that study, *in vitro* bovine blood clots were treated with single-frequency and multi-frequency HIFU. Dual-frequency thrombolysis proved statistically more efficient under identical acoustic power and excitation conditions compared to single-frequency. Notably, no significant difference was found between dual-frequency with different frequency separations (0.025, 0.05, and 0.1 MHz) or between dual-frequency and triple-frequency. In another study, a unique method was described for minimally invasive thrombolysis that combined intravascular forward-looking ultrasound transducers with microbubbles (Kim et al., 2017). A sub-megahertz transducer along with a microbubble injection tube was used in their technology, which was aimed to increase thrombolytic effectiveness and minimize medication requirements. The goal of that arrangement was to improve cavitation-induced microstreaming by overcoming the restrictions of traditional high-frequency, side-looking transducers. Miniaturized transducers capable of generating sufficient pressure for cavitating lipid-shelled microbubbles were developed. *In vitro* experiments demonstrated a promising thrombolytic rate of $0.7 \pm 0.15\%$ mass loss per minute, even without thrombolytic drugs. These findings suggest the potential of this technology for treating thrombotic diseases such as stroke and myocardial infarction. However, further *in vivo* studies are necessary to assess the safety and efficacy of this approach before

clinical implementation. Future research should focus on evaluating potential tissue damage, optimizing treatment parameters, and for confirming the observed benefits in animal models. Dixon et al. (2017) investigated the potential of large-diameter microbubbles with short lifespans for improved sonothrombolysis (Dixon et al., 1965). They employed a microfluidic system to generate large-diameter microbubbles with nitrogen gas cores and non-crosslinked bovine serum albumin shells that ranged in size from 10 to 20 m. These large-diameter microbubbles were delivered directly into a pre-formed clot in a microfluidic channel, replicating *in vivo* proximity delivery. After 1 hour of ultrasonic therapy, large-diameter microbubbles achieved 4.0-8.8- and 2.1-4.2-fold increases in clot lysis, respectively, compared to conventional microbubbles and rtPA alone. These data imply that large-diameter microbubbles applied directly to the clot improved *in vitro* sonothrombolysis effectiveness substantially. However, *in vitro* nature of the study necessitates further investigation to confirm the translation of these results to *in vivo* settings. In another study, they explored the potential of phase-change nanodroplets as a safer alternative to traditional ultrasound-responsive agents in sonothrombolysis (Guo et al., 2019). Utilizing a setup with HIFU, a water tank, and blood clot samples, they investigated the effects of perfluoropentane nanodroplets on clot fragmentation. Compared to HIFU alone, nanodroplet-assisted treatment significantly reduced average clot debris size (from 23.1 μm to 9.8 μm) and the volume percentage of large debris particles (above 10 μm). This suggests that nanodroplets can enhance sonothrombolysis efficacy while mitigating potential tissue damage caused by large debris. However, further research is needed to optimize nanodroplet properties and treatment parameters to fully validate their safety and efficacy *in vivo*. That study highlights the promise of nanodroplets as a potential future direction for safer and more effective sonothrombolysis.

Table 3 summarizes the studies that have been conducted in alternative therapeutic approaches against venous thrombosis in the context of the methodology used, the clot model that was prepared, characterization methods, and the results of those studies.

Table 3. Alternative thrombolytic therapeutic approaches studies.

Author	Thrombolysis Method	Clot Model	Characterization Method	Results
(Suo et al., 2015)	HIFU	Bovine blood + 2.75% W/V CaCl2 (ratio of 10:1 (5 ml/50 ml blood)) - 37C waterbath for 3h	Thrombolysis efficiency = the difference between the clot weights/initial weight	Dual-frequency HIFU is more efficient than single-frequency in thrombolysis efficiency
(Kim et al., 2017)	Ultrasound-enhanced thrombolysis (sonothrombolysis)	Bovine blood + 2.75% W/V CaCl2 (ratio of 10:1 (5 ml/50 ml blood)) - 37C waterbath for 3h	Measuring size difference of clot	After a 40 min treatment, the target clot size reduced to about 35% of its original size (mass reduction from 120
(Dixon et al., 2017)	Microbubble-mediated intravascular sonothrombolysis	Blood + $CaCl_2$ at a concentration of 15 mM (for 4 h at 37 C.) After 4 h, the clots were stored at 4 C for three days to promote clot retraction	Microplate reader	4.0-8.8- and 2.1-4.2-fold increases in clot lysis, respectively, compared to conventional microbubbles and rtPA alone
(Guo et al., 2019)	Phase-change nanodroplets into pulse HIFU	Non-heparinized whole blood from domestic rabbits + Incubation at room temperature for 3 h + Refrigerated at 4 C for 3 d.	Change in clot debris size	In nanodroplets-assisted sonothrombolysis, big clot debris particles (above 10 m in diameter) were smaller, and the average diameter of the clot debris was dramatically decreased.

Even though sonothrombolysis has shown significant potential compared to conventional thrombolytic treatment, it presents drawbacks as a treatment for removing blood clots. One of the drawbacks is the inducement of embolization due to the fragmentation of the clot, which can lead to potential complications (Liu et al., 2018). Additionally, the mechanical vascular impairment and the risk of re-occlusion caused by the activation of platelets are also significant drawbacks of using sonothrombolysis (Liu et al., 2018). Furthermore, sonothrombolysis mostly improves microvascular blood flow without epicardial recanalization, and its feasibility and safety still require further study (Qiu et al., 2022)

1.3. Hydrodynamic Cavitation

Hydrodynamic cavitation is the formation of bubbles in a liquid due to the rapid change in pressure caused by turbulence or flow constriction. When a liquid is subjected to a high-velocity flow or turbulence, the static pressure falls below the saturation vapor pressure of the liquid, leading to the formation of bubbles. Cavitation involves the nucleation, growth, and collapse of vapor or gas-filled bubbles with both destructive and constructive potential. While its uncontrolled occurrence can lead to detrimental effects like corrosion and cell damage, its controlled manipulation presents exciting possibilities in microfluidic-based biomedical applications (Yavuz Perk, 2012). There are two main types of cavitation that have been utilized in biomedical applications – acoustic and hydrodynamic – and explore the unique advantages of harnessing its energy within microfluidic devices.

Acoustic cavitation (AC) utilizes high-frequency sound waves to create and collapse bubbles, generating shock waves with potential for tissue disruption and drug delivery. Hydrodynamic cavitation (HC), on the other hand, exploits rapid flow-induced pressure changes to form and collapse bubbles, resulting in microfluidic flow patterns and forces with potential for cell manipulation and mixing. The cavitation number (Equation (1)), which is defined as a dimensionless number, is extensively used to characterize the intensity of cavitation:

$$\boldsymbol{\sigma = \frac{P_{ref} - P_v}{\frac{1}{2}\rho_1 V_{ref}^2}} \qquad (1)$$

Here, P_{ref} stands for reference pressure, P_{v} represents the saturation vapor pressure of the liquid, ρ_1 is the liquid density, and V_{ref} stands for the reference velocity.

1.3.1. Micro scale Hydrodynamic Cavitation

Microfluidic technology offers distinct advantages in providing controlled cavitation. Compared to traditional scales, the cavitation-on-a-chip approach requires less fluid, enables real-time monitoring and analysis, and allows precise control over bubble nucleation and dynamics (Seyedmirzaei Sarraf et al., 2022). This enhanced control facilitates the study of micro scale cavitation patterns and the manipulation of cavitation-induced forces for specific biomedical applications. Microfluidic devices are becoming increasingly important for studying cavitation at small scales. Pioneering work by (Mishra & Peles, 2005) utilized these devices to explore microscale cavitation, revealing significant scaling effects compared to traditional scales. Notably, surface nuclei play a more prominent role at the micro-scale, leading to a lower inception number. Additionally, cavitating flow patterns rapidly transition to developed and supercavitating regimes, unlike their macro scale counterparts (Ghorbani et al., 2018). Importantly, surface tension forces and stream nuclei residence time are key parameters influencing micro scale cavitation (Ghorbani et al., 2020a) . These findings highlight the unique features of cavitation in small domains and the potential of microfluidic devices for further investigation.

HC in microfluidic systems produces diverse flow patterns, including cavitation clouds, Kelvin-Helmholtz instabilities, and micro vortices (Seyedmirzaei Sarraf et al., 2022). The collapse of these microscale bubbles generates intense shock waves and microjets (Ghorbani et al., 2020b)**.** The inception of cavitation can be affected by surface roughness and instabilities occurring within the flow (Aghdam et al., n.d.). The mechanism of cavitation generation can influence the type of cavitating flow patterns that can be observed and produced. In this context, it is possible to categorize cavitation flow models as inception, non-developed and fully developed cavitation flow models. One of the main factors that causes the transition of non-developed cavitation flow pattern to be developed cavitation is the density of bubble formation. As mentioned, most of the energy released from cavitation comes from bursting bubbles. Therefore, by increasing bubble formation and collapse density, the released energy can also increase. Accordingly, patterns consisting of more bubbles can release more energy. In this context, the released energy can also be controlled by controlling the flow patterns produced. Roughness has an important role in bubble formation intensity and is also provided as a parameter

controlling cavitational flow patterns.

Due to its possible applications in various industries, hydrodynamic cavitation has attracted great interest during recent years. Emerging hydrodynamic cavitation applications include wastewater treatment, food processing, valuable product extraction, biofuel synthesis, emulsification, and waste remediation (Panda et al., 2020). Compared to traditional approaches, the use of hydrodynamic cavitation in these applications offers advantages such as cost effectiveness, reduction of harmful solvent consumption, and the possibility of producing superior processed products (Panda et al., 2020). The collapse of these microscopic cavitation bubbles results in localized hot areas, highly reactive free radicals, and turbulence, all of which can enhance mass transfer, chemical reactions, and mixing processes. Therefore, non-developed cavitation is a possible tool for applications such as chemical synthesis, wastewater treatment and particle size reduction (Gogate, 2010)

HC has been used in various biomedical applications such as cell lysis, deformation, DNA extraction (Namli et al., 2022), cell membrane permeabilization, drug delivery (Gac et al., 2007), and cell sorting/focusing (Wu et al., 2012). Additionally, research on biomedical applications of HC at the micro scale has shown that cavitation has the potential to remove unwanted tissues. (Yavuz Perk et al., 2012) revealed that micro scale HC can be applied for destroying kidney stones. In that study, synthetic kidney stones were exposed to micro scale HC. They discovered that micro scale HC could effectively dissolve stones, with erosion rates increasing as MHC density increases. They then compared cavitation to shock wave lithotripsy, a standard treatment for kidney stones, and discovered that cavitation eroded stones more quickly and with less overall energy input. (Itah et al., 2013) demonstrated that HC treatment resulted in significant tissue ablation leading to reduced prostate size and improved urine flow in benign prostatic hyperplasia tissue in rats. They also discovered that HC treatment was as successful as transurethral resection of the prostate, a commonly used treatment for benign prostatic hyperplasia, in terms of reducing prostate size and increasing urine flow but was less invasive.

HC in microscale presents a promising avenue for various biomedical applications. By harnessing the unique flow patterns and energy release mechanisms of cavitation,

researchers can develop novel tools for undesired tissue ablation, cell manipulation, and drug delivery. Further research in this field holds significant potential for advancing microfluidic technologies and their applications in healthcare.

1.4. Motivation and Novel Aspects

Current therapeutic approaches for thrombolysis, namely conventional treatments and sonothrombolysis, face limitations in terms of efficacy, safety, and energy consumption. In this thesis, micro scale HC was proposed as a more efficient approach for thrombolysis than current therapies due to low energy consumption and highly efficient functionalization. Considering the growing importance of the HC-on-a-chip area in biomedical applications and recent research offer on the importance of surface roughness in generating facile and controlled cavitating flows, incorporating this concept into organ-on-a-chip studies will pave the way for new cutting-edge solutions. To this end, this study aims to present a new platform for the erosion of blood clots using micro scale HC. The platform operates through the coordinated action of two elements: the microfluidic device that precisely controls the occurrence and location of HC to erode the clot, and a polydimethylsiloxane (PDMS) microchip that provides a confined chamber for the retention of a blood clot. Together they form the clot-on-a-chip (CoC) platform. This platform can erode blood clots within seconds by utilizing the micro scale HC. Moreover, the innovative design of the microfluidic device allows for clot erosion at low upstream pressures, significantly reducing the risk of tissue damage during *in vivo* applications. Even though there are studies that have explored acoustic cavitation for clot removal, this thesis represents the first, to my knowledge, to utilize microscale HC within a lab-on-a-chip system for this purpose. Due to the encouraging findings of this study, we envision the development of next-generation, drug-free thrombolysis prototypes utilizing catheter-directed microscale HC technology. This approach certainly holds immense promise for revolutionizing minimally invasive clot removal procedures.

2. HYDRODYNAMIC CAVITATION INDUCED THROMBOLYSIS USING A CLOT ON A CHIP MODEL TOOL

2.1. Experimental Method

2.1.1. Clot-on-a-chip Platform

For the study of clot disruption, a novel Clot-on-a-Chip (CoC) platform (Figure 2) was designed and developed. This platform consisted of two different devices: a silicon microfluidic device and a PDMS microchip. The silicon microfluidic device was designed for the generation of the hydrodynamic cavitation (HC) phenomena in the microscale. PDMS microchip was utilized mainly as a reservoir for the blood clot and as the connection between the silicon microfluidic device and the sandwich holder package. The silicon microfluidic device was aligned precisely on the PDMS microchip and served as the CoC platform. The integrated CoC platform was then positioned within a specifically designed sandwich holder for this system.

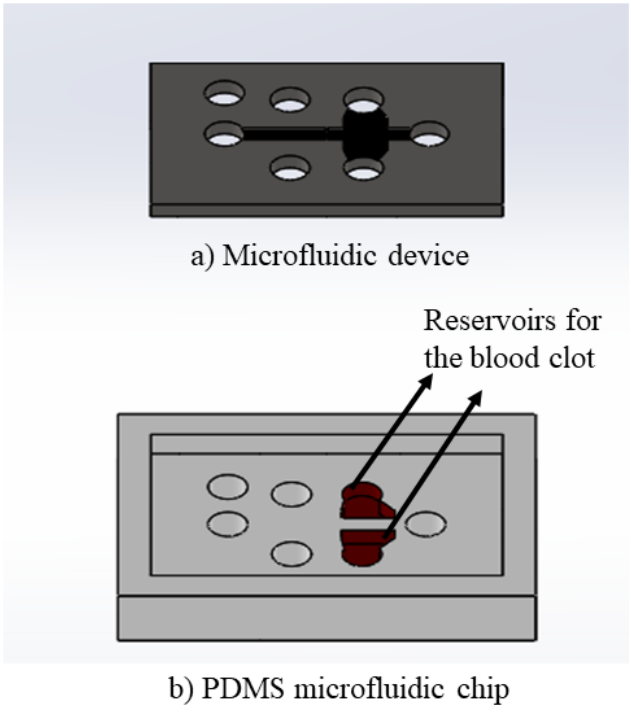

Figure 2. The Clot-on-a-Chip Platform: a) The microfluidic device and b) the PDMS microchip

2.1.2. Microfluidic Device Design and Fabrication

The fabrication procedure and design of the microfluidic device were explained in this section. In general, the microfluidic device was made of a patterned silicon wafer substrate joined by a glass top for visualization. Initially, designs for channels and perforations were transcribed onto acetate paper to serve as masks. Subsequently, a 380 µm thick silicon wafer underwent SiO_2 coating on both sides using a PEVCD device within a cleanroom setting. In the next step, photolithography of specific patterns was taken place using AZ-9221 photoresist. Following that, all microfluidic channels were produced using a deep reactive ion etching (DRIE) procedure to achieve a depth of 50 µm, and a total etching depth of 380 µm for the pressure inlet and the outlet ports. The bottom layer was coated with Ti and Al metals using a Torr Evaporator device to protect the integrity of wafer before full silicon etching. Following these preliminary stages, dry etching was used to finish the microchannel entrances and exits, followed by wet etching to remove the metal coatings. SiO_2 off the surface was removed by wet etching. Following the completion of the silicon preparation, anodic bonding was employed to adhere the silicon wafer to glass. The schematic of the microfluidic device process flow is shown in Figure 3.

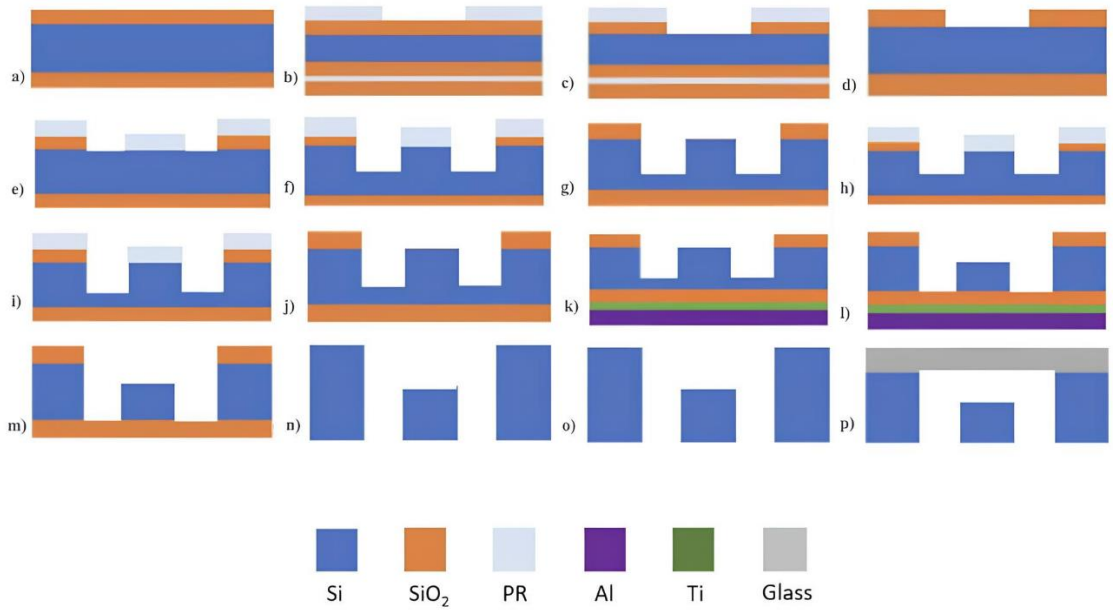

Figure 3. Fabrication procedure of the microfluidic device **a)** Coating both sides of the wafer with silicon dioxide. **b)** Photoresist caoating on a silicon dioxide-coated wafer**. c)** SiO_2 etching **d)** Photoresist removal **e)** Lithography for the inlet–outlet and pressure ports. **f)** DRIE for Si to open

inlet-outler and pressure ports. **g)** Photoresist removal **h)** Photoresist coating and lithography of SiO_2 **i)** DRIE of Si **j)** Photoresist removal **k)** Ti, Al coating. **l)** DRIE for etching through the wafer **m)** Wet etching of Al and Ti **n)** Wet etching of SiO_2 **o)** Cleaning with pirhanna aside **p)** Anodic bonding of the silicon wafer to glass.

The microfluidic device used in this study mainly consists of three parts: the inlet, micro-orifice, and extension (Figure 4). These three locations provide the pressure differential required for bubble nucleation, growth, and implosion cycles. Typically, bubbles occur at the restriction area (Vena Contracta zone) where the flow achieves its maximum velocity. The static pressure rapidly declines as it reaches the pressure recovery zone near the extension area and then begins to climb.

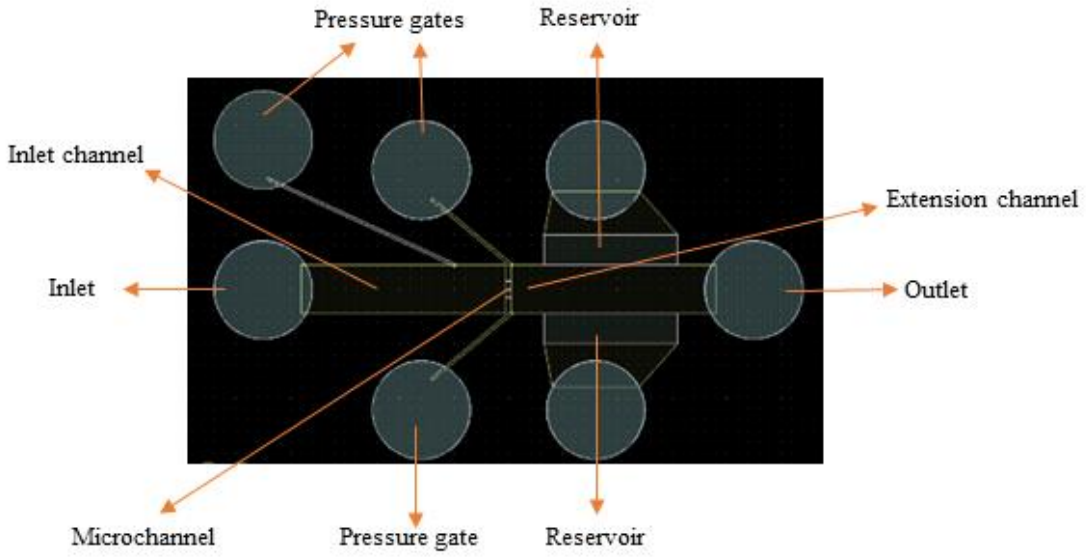

Figure 4. Design of the microfluidic device

To create roughness on the channel surface, a mass flow rate control approach might be used in an optimized DRIE system. The specified roughness structure on the channel surface could be created using sulfur oxide (SF_6) gas, and the gas flow rate could be controlled using mass flow rate. The inlet and extension channels were developed to guide flow within the single microchannel and discharge it out of the microfluidic device. The inlet and extension channels might be 900 and 3750 µm wide and long, respectively. The width, depth, and length of the micro-orifice are tabulated in Table 4. The system enables the formation of shear-induced cavitating flow at lower upstream pressure as the innovative feature of the microfluidic device. Aside from the channels, a microfluidic device has two reservoirs that were designed to inject clots evenly on both sides of the extension channel. Cavitation bubbles are directed to reservoirs, by making use of the

configuration and surface roughness of the microfluidic device as well as makes control of the cavitating flows easier. Furthermore, real-time observation of the channel flow ensured that cavitation bubbles created at the end of the tiny aperture reached the reservoirs.

Table 4. Important dimensions of the microfluidic device geometry.

Physical configuration	Dimension (µm)
Inlet channel length	3750
Micro channel length	100
Clot reservoir length	2450
Reservoir depth	100
Depth	50
Inlet channel width	900
Micro channel width	300
Clot reservoir width	550
Roughness side length	3460

2.1.3. Polydimethylsiloxane Fabrication

The second component of the CoC platform is the PDMS microchip. To ensure precise synchronization and integration within the assembled platform, the microchip molds were designed in Solidworks (2021 Student Edition) software, according to the specific geometrical parameters of both the microfluidic device and the sandwich holder. The resultant mold adopted a rectangular shape with an opening located on the upper surface. Its dimensions were 18.6 mm in length, 13 mm in width, and 2.75 mm in depth. This design also consisted of protrusions for the inlet, outlet, and pressure ports with a 1.8 mm diameter parallel to the microfluidic device. Furthermore, two reservoirs were added to the design with length of 2.45 mm and depth of 870 µm for the placement of the blood clot. Additionally, a recessed area with smaller dimensions was incorporated into the design to facilitate accurate placement and alignment of the microfluidic device within the PDMS microchip. This zone is measured 8.40 mm in height, 14 mm in length, and 0.88 mm in depth. Notably, the PDMS microchip mold dimensions surpassed those of the microfluidic device to compensate for shrinkage that typically occurs during the PDMS curing process within the mold. This deliberate design allowed the perfect alignment of the microfluidic device within the PDMS microchip, thereby maximizing the

functionality of the CoC platform. Later, molds of the PDMS microchips were fabricated using a 3D Printer (Ultimaker S3).

In each production, six molds of the PDMS microchips were fabricated with the same design of the PDMS microchip mold. An exact weight ratio of 10:1 was utilized between the elastomer base and the curing agent (SYLGARD™ 186 Silicone Elastomer Kit) for the fabrication of make PDMS microchips and the components were thoroughly mixed for 10 minutes. To eliminate any entrapped air bubbles from the mixture, vacuuming was performed. The de-aerated slurry was then gently poured into PDMS chip molds. The molds were then placed in an oven which was set at 80°C for curing. In the small-sized molds, the PDMS polymer was cured for 2 hours. After allowing the PDMS microchips to cool to ambient temperature, they were taken from the mold and cleaned with ethyl alcohol and deionized water. The schematic illustration of PDMS microchip is shown in Figure 5.

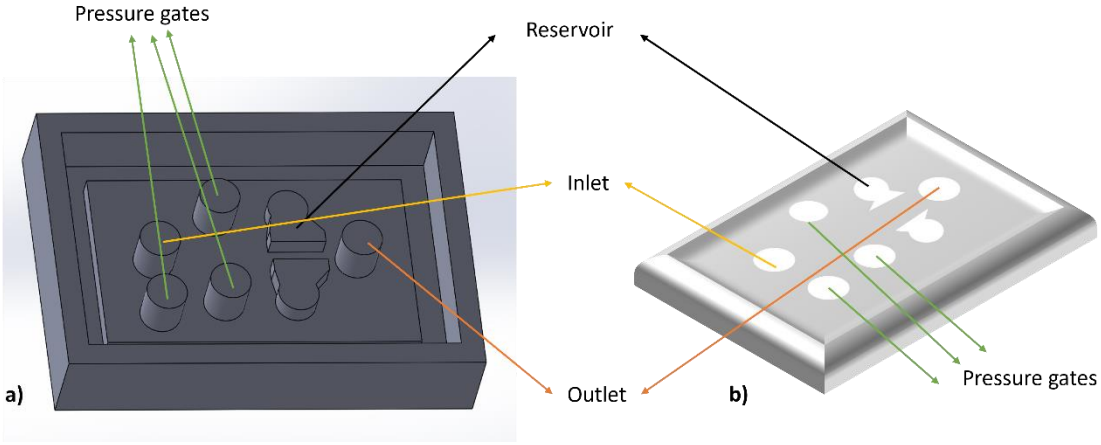

Figure 5. Schematic of the design of the **a)** PDMS microchip mold **b)** PDMS microchip

2.1.4. Sandwich Holder Package

A specialized sandwich holder was developed in parallel to the CoC platform. The microfluidic device and PDMS microchip were held together via the sandwich holder. Furthermore, this developed sandwich holder provided the connection between the CoC platform and experimental setup. A single inlet for fluid supply from a container and a single outlet for fluid flow exiting from the microfluidic device was included in the sandwich holder. The inlet and output are both 10 mm in diameter. The geometrical

information about the silicon microfluidic device and tubing system connected to the experimental setup were used to determine the dimensions of the sandwich holder. The sandwich holder had an octagonal shape with a width of 80 mm, a length of 80 mm, and a height of 20 mm. It was made sure to have exact alignment and placement of the CoC system, which allowed for its integration to the experimental setup. In Figure 6, both the design of the sandwich holder with important dimensions and the schematic of the sandwich holder are shown.

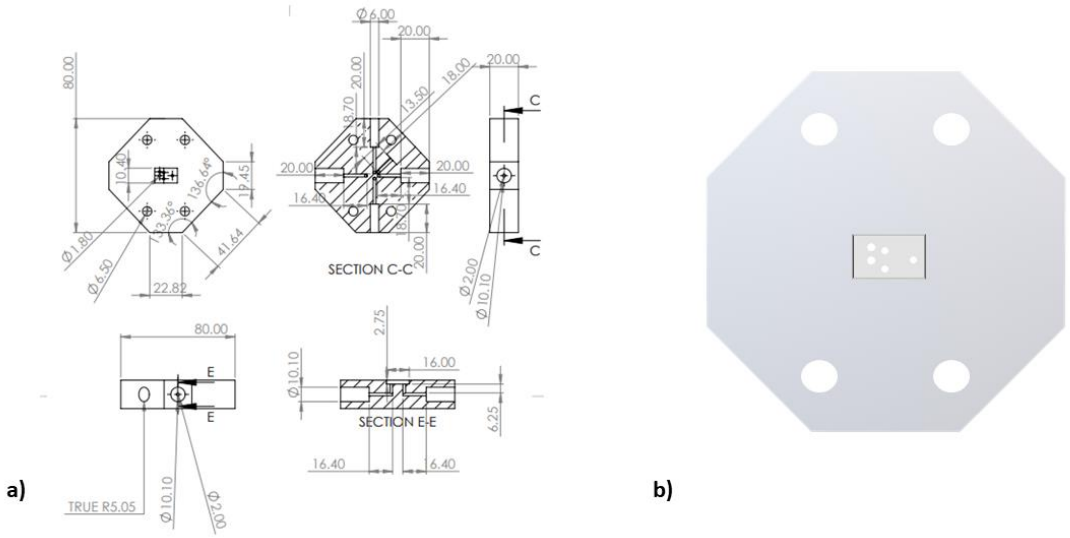

Figure 6. Sandwich holder package **a)** Design of the sandwich holder with important dimensions. **b)** Schematic of the sandwich holder.

2.1.5. Experimental Setup

The experimental setup, which is illustrated in Figure 7, is composed of a high-pressure pure nitrogen tank (Linde Gas, Gebze, Kocaeli, Turkey), a fluid container (Swagelok, Erbusco BS, Italy), stainless-steel tubing, T-type filter (Swagelok) with a nominal size of 15 µm, Omega pressure gauges (Omega, Manchester, UK, with an accuracy of 0.25% and a range of up to 3000 psi), a sandwich holder, the microfluidic cavitation on a chip device, the PDMS microchip, a high-speed double-shutter CMOS camera (Phantom VEO-710L), a macro-camera lens (model K2 DistaMax) and a beaker.

In this thesis, a fluid container was connected to a high-pressure pure nitrogen tank which forced distilled water through stainless-steel tubing through the experimental apparatus.

Omega pressure gauges were used to measure pressure. To eliminate undesirable particles from the working fluid, a T-type filter was also utilized. The microfluidic device and PDMS microchip were placed inside the sandwich holder which was mounted between two plexiglass packages to allow flow visualization. The sandwich holder had one inlet connected to the fluid container and one outlet for fluid exiting the microfluidic device. To prevent leakage in the system, tight connections were employed. Consequently, the final configuration had a sequential arrangement of a sandwich holder, a PDMS microchip with blood clot inside, and a microfluidic device, two plexiglass packages from the bottom to the top layers. During the experiments, the cavitating flow patterns were captured using a high-speed double-shutter CMOS camera that was connected to a computer with a resolution of 1280 × 800 pixels with 0.02 mm pixels. A macro-camera lens with a focal length of 50 mm and a f-number of 1.2 was also utilized. To assist in visualization, the camera system was situated 200 mm distant from the experimental setup, which ensured that it was aligned with the focus area and only recording images from the core region of the lens. With a shutter speed of 1000 s^{-1} and an exposure duration of 1 s, the camera recorded high-speed flow images at a frame rate of 12,200 fps. To provide appropriate illumination in front of the microdevice and to increase visibility, a point halogen light source was employed.

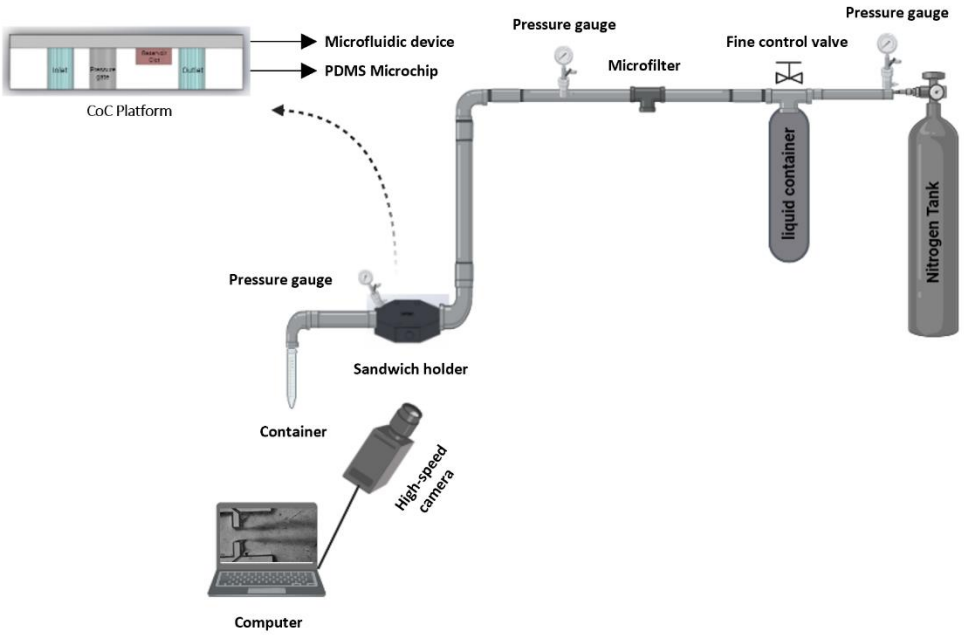

Figure 7. Schematic of the experimental setup with the CoC platform.

2.1.6. Blood Clot Sample Preparation

Blood was drawn into 2 mL tubes containing 3.2% sodium citrate to prevent clotting. Subsequently, 500 µL of blood was transferred to a 2 mL Eppendorf tube using a micropipette. To initiate coagulation, 50 µL of 0.5 M Calcium Chloride (MERCK KgaA, Darmstadt, Germany) solution was added to the blood at a 1:10 buffer-to-blood ratio in fume hood. The mixture was then gently mixed for 10 seconds to ensure homogenous distribution of the calcium ions. For clot formation, the blood samples were incubated for 4 hours in water bath preheated to 37°C, which simulated physiological body temperature. After the clot formation, the blood clot was immediately retrieved and inserted into the PDMS microchip mold for subsequent hydrodynamic cavitation exposure. This procedure aimed to minimize the handling time of the clot to preserve its structural integrity and to prevent potential artifacts during the cavitation process. The schematic of blood clot preparation is shown in Figure 8.

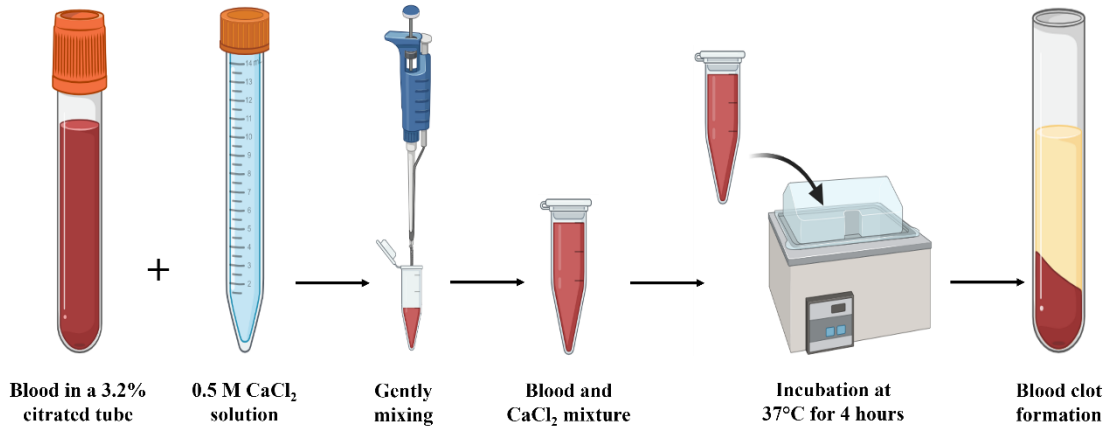

Figure 8. Blood clot preparation protocol

2.1.7. Hydrodynamic Cavitation Experiments

2.1.7.1. Hydrodynamic Cavitation Experiments with CoC Platform

Before the experiments, the integrity of the CoC platform was evaluated. To ensure that no fluid leakage occurred during operation, a system leakage test was conducted. The CoC platform was assembled without the blood clot and secured within the sandwich holder. The system was connected to the experimental setup, and the inlet pressure was gradually increased via the pure nitrogen tank. Distilled water was subsequently propelled

through the stainless-steel tubing and flowed through the microfluidic channels of the CoC platform. This process confirmed the absence of any leaks within the system. Furthermore, to verify the functionality of the CoC platform for HC experiments, a visualization study was conducted. For this, the integration of a designed and fabricated microfluidic device with a PDMS microchip was made. The platform was connected to a high-speed camera, which allowed real-time visualization of both the microchannel and the extension channel of the microfluidic device. By gradually increasing the pressure within the system, the initiation and development of the HC phenomenon were observed within the microfluidic channels of the CoC platform. This visualization confirmed the suitability of the CoC platform for subsequent HC treatment experiments.

2.1.7.2. Hydrodynamic Cavitation Treatment to the Blood Clot

Six PDMS microchips were fabricated from identical molds for hydrodynamic cavitation treatment. Each blood clot was carefully placed within the reservoir of a dedicated PDMS microchip. The same microfluidic device was used in every set of experiments. After integrating the microfluidic device and the corresponding PDMS microchip, the complete CoC platform was secured within the designed sandwich holder. The sandwich holder was then connected to the experimental setup for controlled cavitation treatment. Each blood clot was treated with a specific set of conditions which are listed in Table 5.

Table 5. The hydrodynamic cavitation treatment conditions applied to each blood clot.

Set of Experiments	Pressure (psi)	Exposure Time (s)
PDMS microchip 1 + Blood Clot 1	70	30
PDMS microchip 2 + Blood Clot 2	70	60
PDMS microchip 3 + Blood Clot 3	70	90
PDMS microchip 4 + Blood Clot 4	70	120
PDMS microchip 5 + Blood Clot 5	25	120
PDMS microchip 6 + Blood Clot 6	10	120

The first blood clot received 120 seconds of treatment at 70 psi pressure, 70 psi was selected since the fully developed cavitation was observed at this pressure. The second blood clot was treated for 90 seconds at the same pressure. The third blood clot had 60 seconds of treatment at 70 psi pressure, and the fourth blood clot received 30 had at the

same pressure. For the fifth blood clot, the treatment time was 120 seconds, but the pressure was reduced to pressure of 25 psi since cavitation incepted at the pressure of 25 psi. Finally, the sixth blood clot had the 120 seconds treatment time, but at the pressure of 10 psi which corresponded to no hydrodynamic cavitation which implied that only the fluid flow effect on the blood clot exists. Following each treatment, the sandwich holder was removed from the setup, and the treated blood clot was carefully extracted for further analysis. This process was repeated for all six PDMS microchips, to have consistent treatment analysis for each individual blood clot.

Regarding the analysis of mass change in each blood clot, each PDMS microchip and the blood clot mass were weighted using an analytical balance (Sartorius CPA 224 S Balance, 220g x 0.1 Mg) both before and after the HC treatment. Also, the PDMS microchip was exposed to HC treatment solely without placing the blood clot to only measure the water retention amount of the PDMS microchip. This amount was later extracted from the PDMS microchip and blood clot mass while analyzing the change in mass of blood clots. For the analysis of the diameter change of each blood clot, blood clot images were taken with digital camera both before and after the HC treatment. The diameter change in blood clots was analyzed using images taken both before and after the HC treatment by the ImageJ Software. Summary of the experimental procedure is illustrated in Figure 9.

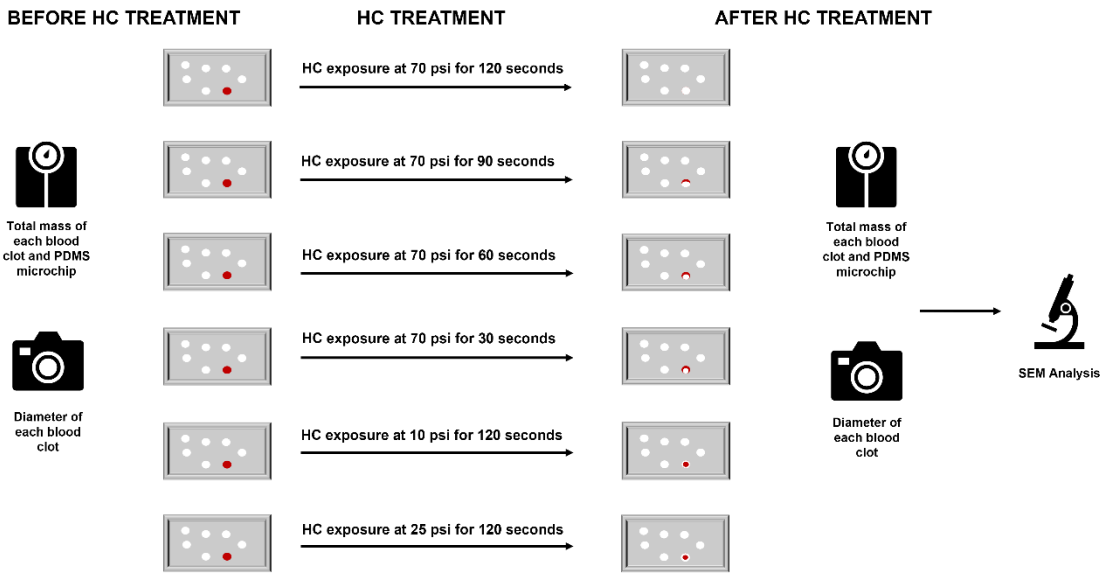

Figure 9. Schematic summary of the experimental procedure

2.1.8. Scanning Electron Microscopy Characterization

After HC treatment, the human blood clot samples (for scanning electron microscopy (SEM) analysis) were prepared in a fume hood by following a protocol adapted from (Petit et al., 2012). In a controlled environment, the samples underwent a brief triple wash in a phosphate-buffered saline (PBS) solution (Sigma Aldrich, 524650). Subsequently, they were fixed at room temperature for 18 hours in a 2.5% glutaraldehyde solution (Sigma Aldrich, 49629). Following fixation, the samples had another two PBS washes for 5 minutes, each to eliminate residual glutaraldehyde from the clots. Dehydration of the specimens was accomplished using varying concentrations of ethanol, namely 1.8%, 10%, 20%, 40%, 50%, 70%, 80%, 90%, and two subsequent immersions in 100%, each exposure lasting 2 minutes. The dehydrated samples were allowed to rest for 24 hours at room temperature inside the fume hood for 24 hours. Before SEM imaging, the samples were coated for three times with a layer of Au-Pd to facilitate electron transfer (Denton Vacuum, Desk V). Then, the morphology of the samples was imaged using a field-emission scanning electron microscope (SEM; Zeiss LEO Supra 35 VP) operated with an accelerating voltage of 3 kV at magnifications of 5000, 10000 and 20000. Later, the mean diameter of cavities appearing on blood clots were measured from SEM micrographs using the ImageJ Software.

2.1.9. Statistical Analysis

All experiments were performed at least for three times. The mean values, standard deviations and standard error values of all obtained results were obtained. Relationships among groups were analyzed using one-way ANOVA (GraphPad Prism 5.01), [Tukey's multiple comparison test (* p\0.05, ** p\0.01, *** p\0.001)].

3. RESULTS

3.1. Cavitating Flow Inception

Cavitation inception, the initial formation of microscopic bubbles in the liquid, was generally observed at lower pressures within the microfluidic device. In the context of clot removal, this inception point marked the application of hydrodynamic forces via these bubbles. Sudden pressure drops within the microfluidic channels, attributed to sidewall surface roughness and specific design parameters, were responsible for their creation. The intricate channel geometry facilitates rapid pressure fluctuations, creating the necessary conditions for inception. Observing and understanding this phenomenon is crucial for effective clot removal. Using a high-speed camera, cavitation inception was detected at the pressure of 25 psi in the utilized microfluidic device (Figure 10). This event initiated a cascade of effects. The newly formed bubbles create a low-pressure zone, high-turbulence environment. These bubbles act as initiators of the erosion process, which facilitated the mechanical disintegration of the clot. Their presence contributes to the formation of dense microfluidic flow zones and high-shear stress regions. These localized forces are responsible for the fragmentation of the clot. Essentially, cavitation inception lays the groundwork for the subsequent clot removal via a combination of bubble-induced erosion and high shear stresses generated within the microfluidic channels.

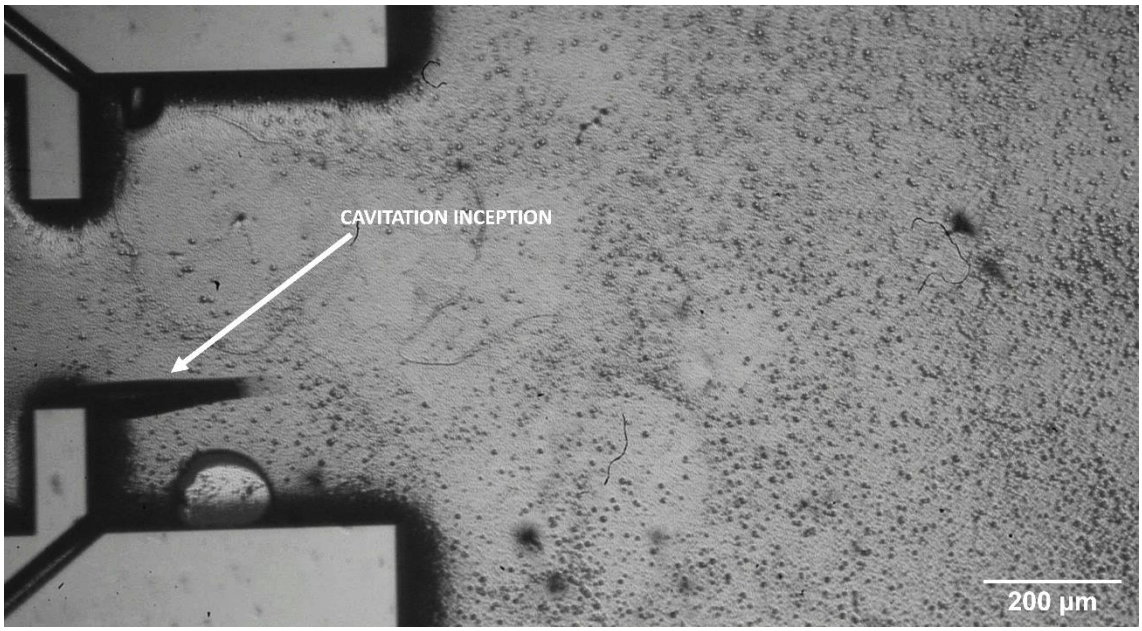

Figure 10. Cavitation inception (25 psi) inside the utilized microfluidic device beginning from microchannel to extension channel conditions.

While cavitation inception highligted the initial bubble formation within the microfluidic device, fully developed cavitation, observed at the pressure of 70 psi in Figure 11, represents a more advanced stage in the cavitation process. This transition from emerging bubbles to robust cavitation clouds is primarily driven by two parameters: structural roughness within the microfluidic chip and the comprehensive design parameters that govern pressure fluctuations. As the pressure within the device surpasses the initial cavitation threshold, the microscopic bubbles forming during inception evolve and expand, transform into larger, and more stable cavitation clouds. These clouds exert significant forces on the surrounding liquid, which plays a crucial role in the context of clot removal. Unlike the initial localized effects of cavitation inception, fully developed cavitation was on a more aggressive role. The intense forces generated by the cavitation clouds induce rapid and significant erosion on the clot. This erosion manifests itself as severe degradation, disintegration, and fragmentation of the clot structure. This potent combination of bubble-induced erosion and pressure-driven forces make fully developed cavitation a vital tool in achieving efficient clot removal within microfluidic devices.

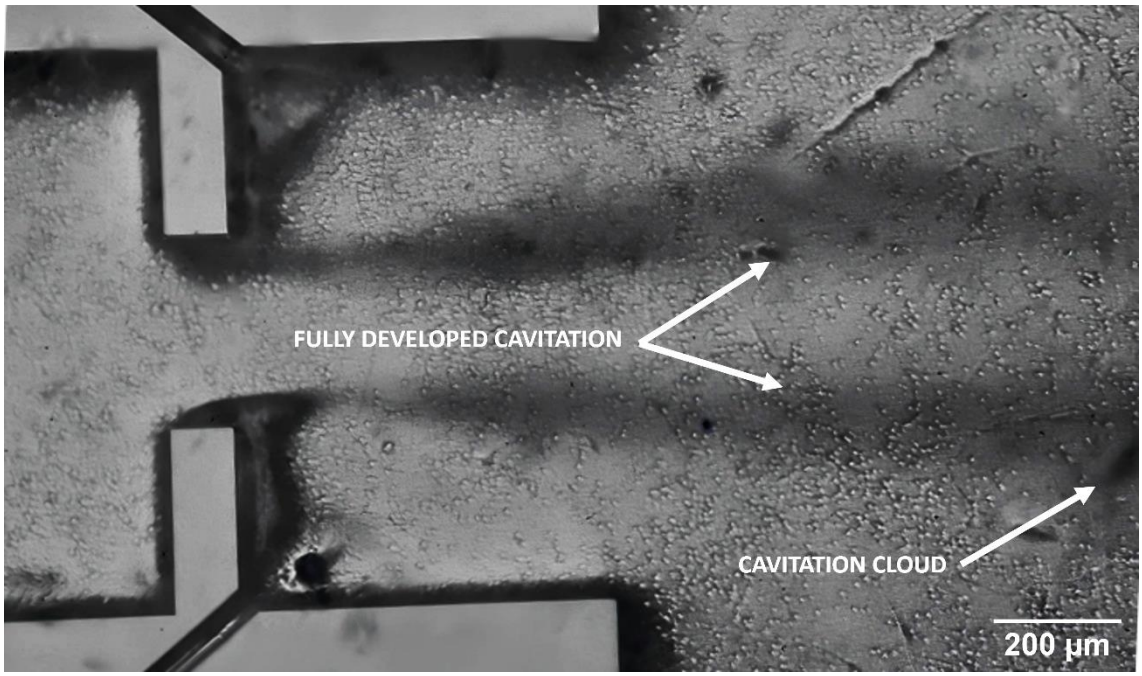

Figure 11. Fully developed cavitation (70 psi) inside the microfluidic device beginning from the microchannel to extension channel occurrence.

The presence of structural sidewall roughness implemented in chip designs created favorable conditions for cavitation bubbles to form at low pressures. This phenomenon was specifically attributed to the unique design of the chip architecture, which causes cavitation to occur even at relatively low pressures (25 psi). The transition from initial cavitation to fully developed cavitation is an important factor on clot removal process. During this transition, the effectiveness of the approach was obtained at a high level in repeated experiments.

3.2. Cavitating Flow Exposure to Blood Clot

In this section, the critical role of in-chip pressure measurements in understanding the cavitation process and its effectiveness in clot removal was demonstrated. These measurements were useful in finding pressure drops within the microfluidic device, a key parameter for triggering cavitation. At 25 psi inlet pressure, the microchannel exit pressure dropped to 8 psi, corresponding to a Reynolds number of 239 and a cavitation number of 35.1. These values indicated a bubbly cavitation stage with microscopic

bubbles. As the inlet pressure increased to 70 psi, the microchannel exit pressure rose to 20 psi. Consequently, the Reynolds number increased to 3818.4 and the cavitation number dropped to 0.486. These values signified a transition to fully developed cavitation with larger, and more stable cavitation clouds.

The modest pressure drop within the microfluidic device facilitates precise control over the cavitating flow, and implies directing it towards the designated clot reservoir locations. The proposed design innovation enables targeted fluid manipulation within the device. Specifically, the side-wall roughness implemented downstream of the cavitation zone, induces the formation of elongated cavitation "clouds." These clouds, as observed in the first image of Figure 12, generate vortices that move inwards towards the reservoir voids. These vortices release significant energy due to their entrained bubbles.

The cavitation-generated energy is effectively channeled towards the clot nests within the reservoirs, which promoting progressive clot erosion over time. Figure 12c displays a sequence of high-speed camera captures which, showcase the cavitation vortex entering the reservoirs and air bubbles exiting alongside eroded clot particles. This mechanical surface erosion is a direct consequence of the cavitation vortex transporting bubbles onto the clot surface. Unable to withstand this erosive force, the clot particles are gradually dislodged and carried away by the flow towards the outlet.

Interestingly, the air bubbles generated at the site of clot erosion are swept back towards the vortex origin (microchannel outlet) by the same cavitating flow. These bubbles then re-enter the cavitation cycle, contributing to a self-sustaining loop.

The unique design of the silicone-glass device, coupled with the optimized design parameters and side-wall roughness effectively initiates and targets towards the reservoirs, where it is transformed into a high-energy vortex. Figure 12 further illustrates impact of the study on the clot surface over time and under varying pressure conditions.

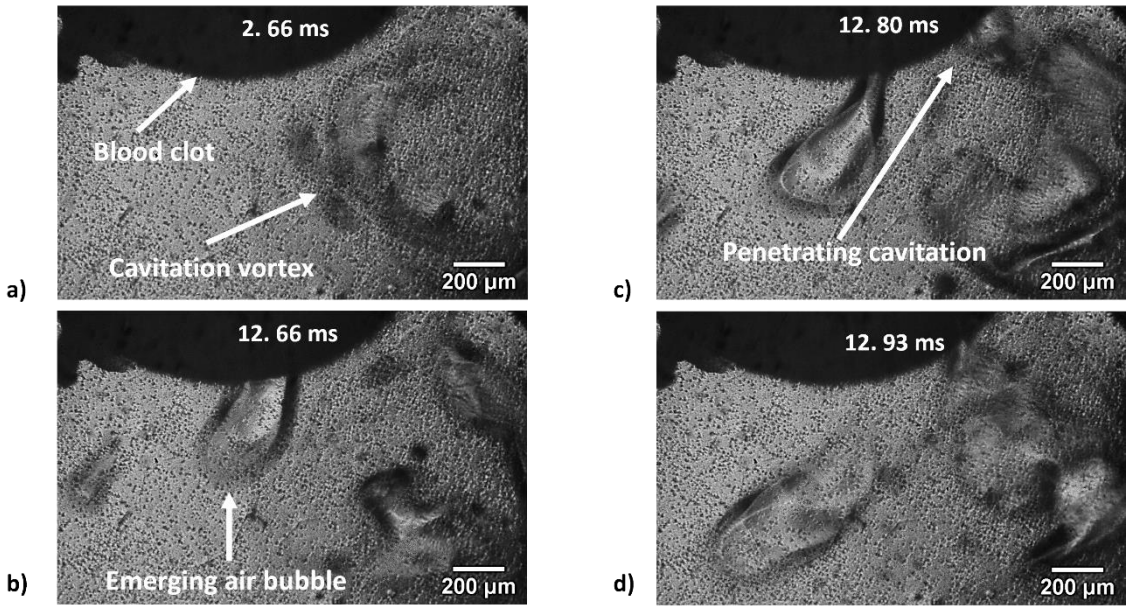

Figure 12. Cavitation targeted to blood clot visualization of the CoC platform with a high-speed camera. **a)** Cavitation vortex at 2.66 ms. **b)** Emerging bubble at 12.66 ms. **c)** Penetrating cavitation to the blood clot inside the reservoir at 12.80 ms. **d)** HC phenomenon direction to a blood clot at 12.93 ms.

3.3. Change in Physical Properties of Blood Clot

3.3.1. Mass Change of Blood Clot

The change in mass of blood clots was determined by measuring both before and after the experiment of total mass of the PDMS microchip with blood clots inside its reservoirs for three experiments (Table 6).

Table 6. Mass change of blood clots.

		Change in the blood clot mass (mg)			
Pressure (psi)	**Exposure Time (s)**	**Experiment 1 (mg)**	**Experiment 2 (mg)**	**Experiment 3 (mg)**	**Erosion rate (mg/s)**
10	120	3.7	4.3	2.7	0,0297
25	120	4	4.4	4.1	0,0347
70	30	4.2	4.7	4.4	0,1477
70	60	4.7	5	5.2	0,0827
70	90	5.6	5.5	6.1	0,063703704
70	120	5.9	6.2	6.3	0,051111111

The results reveal that the most significant mass change occurred at the pressure of 70 psi for the exposure time of 120 seconds when considering all three experiments (with 6.1±0.2 mg). This finding aligns with the occurrence of fully developed cavitation at this pressure, which causes the most destructive force on the clot compared to other cases. The next most significant mass change is observed at the pressure of 70 psi for 90 seconds with 5.7±0.32 mg. This finding further supports the link between fully developed cavitation and substantial clot disruption. Although the exposure time is shorter in this case compared to the 120-second experiments, the pressure remains at the critical threshold for having the maximum cavitation effect. The least change in mass is obtained at the pressure of 10 psi for 120 seconds with 4.5±0.8 g. This is attributed to the absence of HC at this pressure which results in minimal clot disruption. Furthermore, at a constant pressure, the change in mass decreases with decreasing exposure time while, all the results obtained from three experiments (at a constant exposure time), the change in mass increases with increasing pressure. These findings are shown in Figure 13. Further, this outcome provide valuable insights into the relationship between HC parameters and the effectiveness of clot disruption.

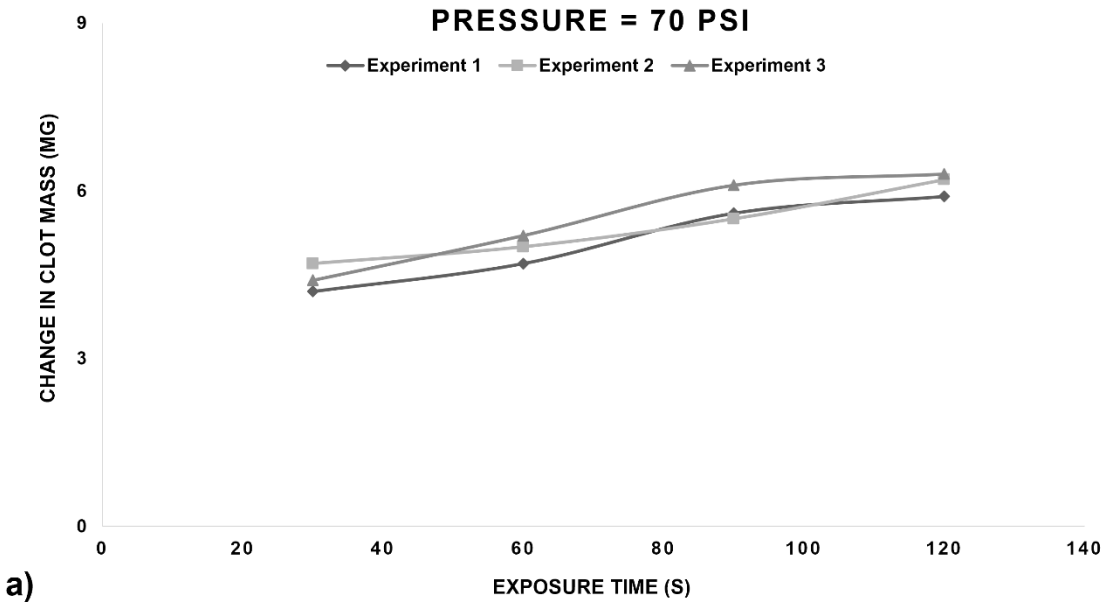

a)

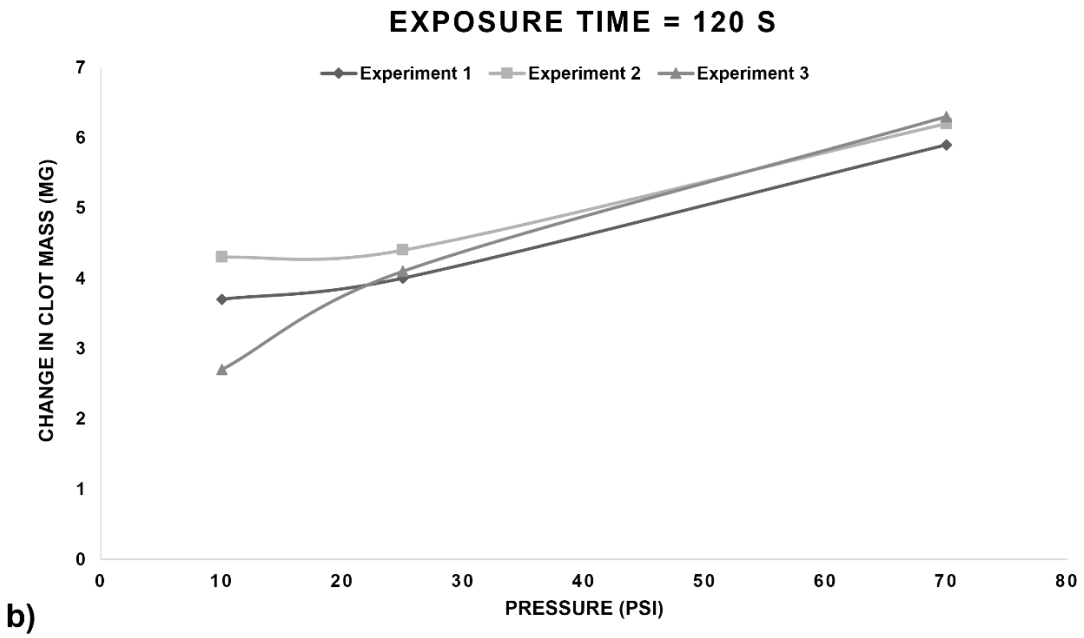

Figure 13. Mass change of blood clots with time for three experiments

The erosion rate of blood clots under various HC condition defined as the mass change per second of the clots. Erosion rate is displayed in Figure 14. Accordingy, the control group lead to the least erosion rate observed at 10 psi pressure for 120 seconds with 0.029 mg/s. The highest erosion rate is attained at 70 psi pressure for 30 seconds with 0.147 mg/s. Notably, at constant 70 psi pressure, the erosion rate progressively decreases from 30 seconds to 120 seconds. This finding suggests that while fully developed cavitation promotes initial significant erosion of blood clots during HC treatment, its effect diminishes over time. Furthermore, the erosion rate trend aligns with the cavitation inception pressure results, where 25 psi for 120 seconds (less than the fully developed cavitation pressure of 70 psi) yields lower erosion rate with 0.034 mg/s as anticipated due to less intense cavitating flow associated with incipient cavitation.

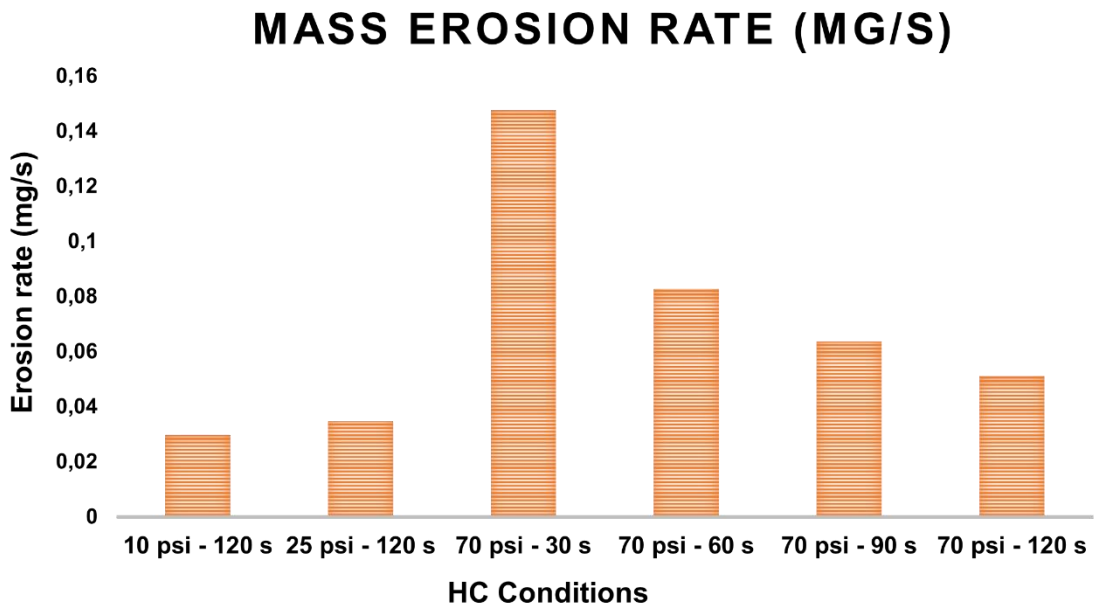

Figure 14. Erosion rate of blood clots under different HC conditions based on the mass change over time.

3.3.2. Diameter Change of Blood Clot

For all the experimentals, the change in diameter of blood clots was determined by acquiring images of blood clot inside the PDMS microchip and analyzing then using the ImageJ software. The changes in diameter of blood clots in each experiment are shown in Figure 15.

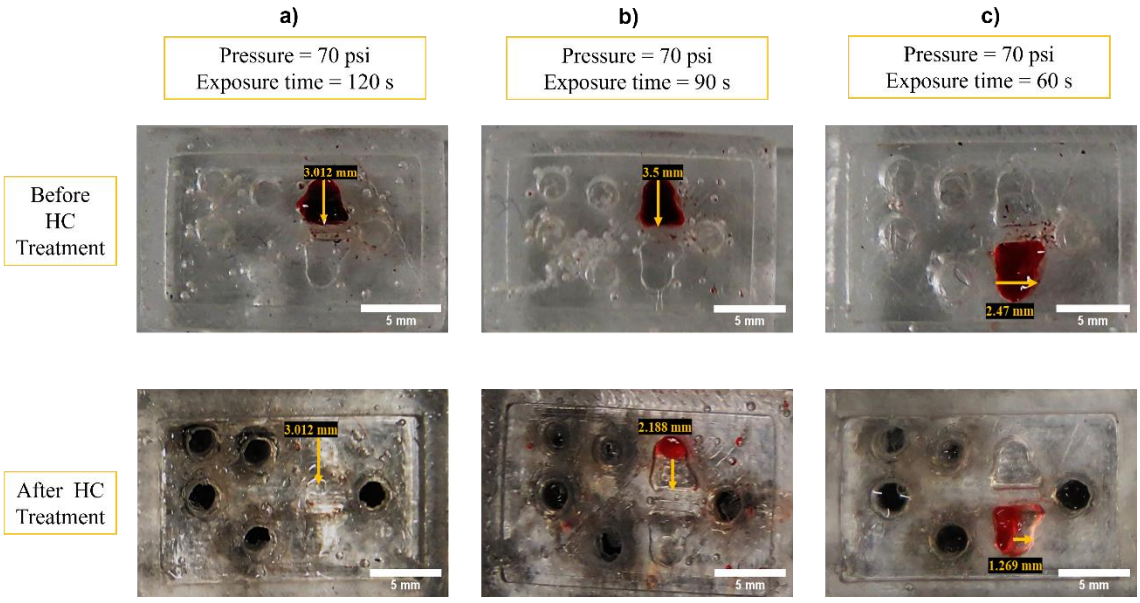

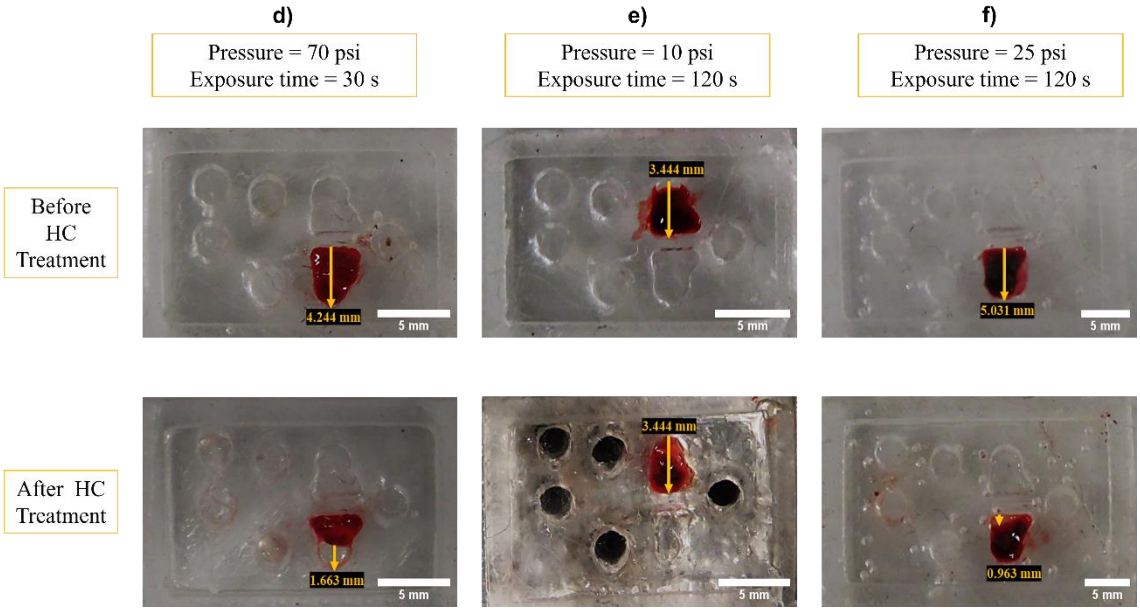

Figure 15. Diameter change of blood clots upon HC treatment a) at 70 psi for 120 s b) at 70 psi for 90 s c) 70 psi for 60 s d) 70 psi for 30 s e) 10 psi for 120 s f) 25 psi for 120 s.

According to the results, the most significant erosion occurs at the pressure of 70 psi for 120 seconds. This case is able to dissolve the blood clot. This observation coincides with the presence of fully developed cavitation at this pressure, which is due to the most powerful disruptive force on the clot compared to other parameters. The second most significant erosion is observed at the pressure of 70 psi for 90 seconds, with a 62.5% reduction in diameter. This finding further strengthens the link between fully developed cavitation and substantial clot erosion. Despite the shorter exposure time compared to the 120-second experiments, the pressure remains at the critical threshold for the maximum cavitation effect. At the pressure of 70 psi for 60 and 30 seconds, the erosion percentages are 51.4% and 39.2%, respectively. These results demonstrate that increasing pressure at constant exposure time leads to a larger blood clot diameter loss. The least erosion is obtained at the pressure of 10 psi for 120 seconds, where no measurable erosion occurs. This further supports the conclusion that HC is effective in clot disruption while the effects are minor in the subsence. The loss in diameter was less (19.1%) for treatment at the pressure of 25 psi for 120 seconds, indicating that less erosion occurs under the cavitation inception condition. All of the results are included in Table 7.

Table 7. Diameter change of blood clots.

		Diameter of blood clots		Change in diameter of blood clots		
Pressure (psi)	**Exposure Time (s)**	**Before HC Treatment(mm)**	**After HC Treatment (mm)**	**Change (mm)**	**Percentage (%)**	**Erosion Rate (µm/s)**
10	120	3,444	3,444	0	0	0
25	120	5,031	2,355	0,963	19,1	6.2
70	30	4,244	1,586	1,663	39,2	35.5
70	60	2,47	1,005	1,269	51,4	17.9
70	90	3,5	1,694	2,188	62,5	21.0
70	120	3,012	0	3,012	100	28.7

The erosion rate of HC conditions, per second. The diameter change is divided by the time to get the erosion rate and depicted in Figure 16. Accordingly, the control group, characterized by the absence of cavitation at 10 psi pressure for 120 seconds, has no measurable erosion. In contrast, the highest erosion rate is observed at 70 psi pressure for 30 seconds with 35.5 µm/s. Interestingly, at a constant pressure of 70 psi, the erosion rate continuously increased with exposure time (for 60, 90 and 120 seconds 17.9 µm/s, 21.0 µm/s and 28.7 µm/s, respectively).

This finding suggests that, in spite of inducing significant initial erosion, fully developed cavitation does not sustain its erosive potential over longer HC treatment durations. Furthermore, the observed relationship between erosion rate and cavitation pressure reinforces the notion that lower pressure exposures and less intense cavitation, produce correspondingly less erosion. All these findings agree with those of erosion rates based on the mass change.

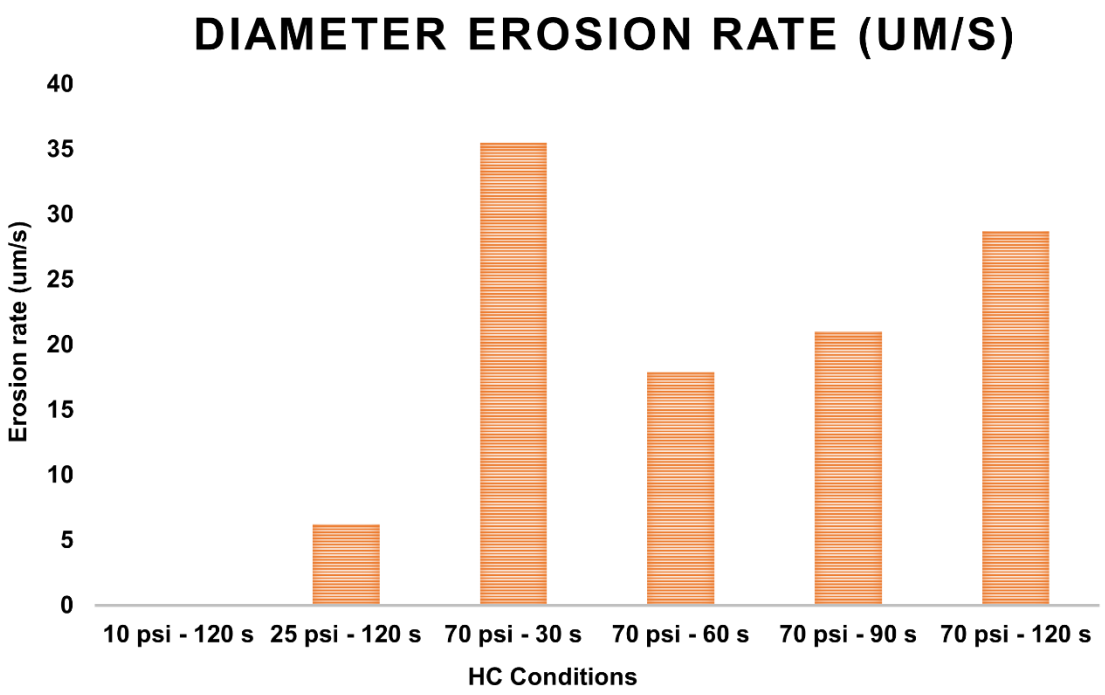

Figure 16. Erosion rate of blood clots in different HC conditions depending on the diameter on the diameter change

3.4. Change in Biological Properties of Blood Clot

3.4.1. Scanning Electron Microscopy Analysis

Scanning electron micrographs of human blood clots are shown in Figure 13. SEM images reveal that the clots are generated by red blood cells, fibrin, and platelets, the three primary elements of *in vivo* clots (Maegerlein et al., 2018). In this part, blood clots were subjected to HC treatment at varying pressures and durations, and the resulting morphological changes were examined. The first column of Figure 13 represents the control group, where blood clots were not exposed to HC treatment. HC treatments at the pressure of 25 psi for 120 seconds, at the pressure of 70 psi for 30 seconds, and at the pressure of 70 psi for 90 seconds are shown in the second, third, and the fourth columns, respectively. The magnification of the micrographs from (5000 X to 20000 X) increases from the first row to the third row.

SEM micrographs (Figure 17a, e, i) show intact red blood cells and a well-preserved network of fibrin fibers. This confirms the presence of a proper and undisturbed blood

clot structure. The second column depicts the effects of HC treatment at the inception pressure (25 psi for 120 seconds). While the SEM micrographs (Figure 17b, f, j) still include largely intact red blood cells, some initial damage to fibrin fibers becomes evident. The fibers appear as slightly distorted and disconnected in isolated areas, which suggests the onset of clot erosion. Furthermore, HC treatment at the fully developed cavitation pressure point (70 psi for 30 seconds) leads to more severe damage, as illustrated in the third column (Figure 17c, g, k).

At this stage, SEM micrographs indicate a significant loss of connections between fibrin fibers, accompanied by the initiation of red blood cell lysis due to mechanical stress inflicted by HC treatment. The most severe damage occurs in the fourth column, which represents HC treatment at the pressure of 70 psi for 90 seconds. The SEM micrographs (Figure 17d, h, l) reveal the loss of clot integrity due to widespread breakage of fibrin fibers and extensive red blood cell lysis. These results clearly demonstrate that the microstructural damage is inflicted on blood clots by HC treatment. Notably, SEM images directly mirror the trends observed in erosion rates based on both mass and diameter changes. As HC intensity increases (reflected by pressure and duration, from inception and developed cavitation), both microstructural damage and physical property changes become progressively more visible.

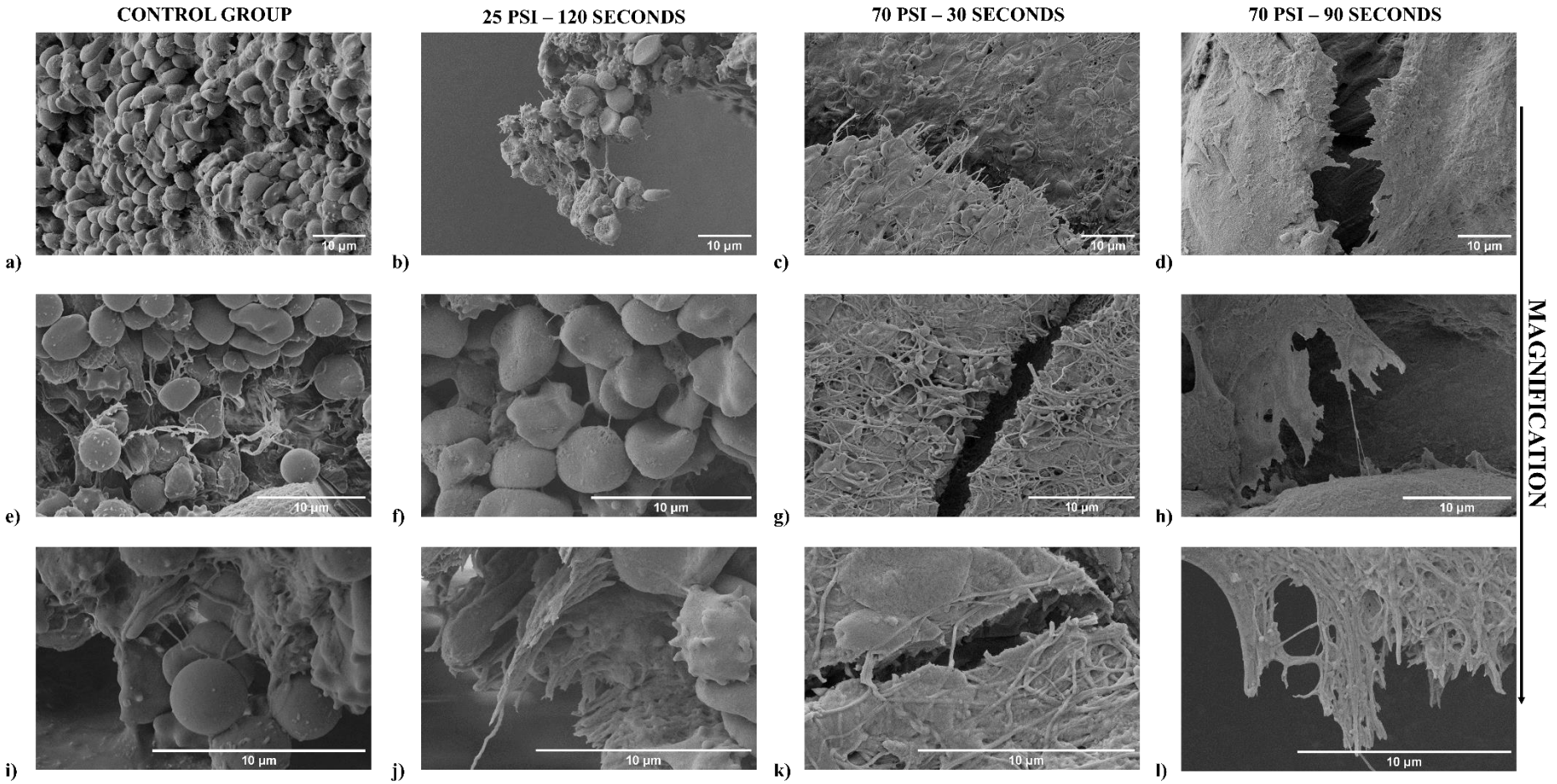

Figure 17. SEM images of blood clots **a, e, i)** Control group with 5 X, 10 X, 20 X. **b, f, j)** HC treatment at 25 psi (cavitation inception) for 120 s with 5 X, 15 X, 20 X. **c, g, k)** HC treatment at 70 psi (fully developed cavitation) for 30 s with 5 X, 10 X, 20 X. **d, h, l)** HC treatment at 70 psi (fully developed cavitation) for 90 s with 5 X, 15 X, 20 X. magnification from first row to third row, respectively.

Figure 18 presents SEM images of human blood clot surfaces subjected to various HC treatment. The first column (Figure 18a, e) depicts clots treated at 10 psi for 120 seconds, which represent the control group with no HC cavitation. The second and third columns showcase clots exposed to fully developed cavitation pressure of 70 psi for 30 and 60 seconds, respectively. Magnification is consistently increased from 10,000x to 20,000x across the rows. Cavities generated by HC exposure are visualized. The control group (Fig18.a, e) leads to minor cavity formation, evidenced by a mean area of 0.108±0.125 μm^2. This signifies minimal damage to the clot structure, which implies the hypothesis that HC cavitation is the responsible factor for clot deformation.

The second column micrographs (Figure 18b, f) reveal evident surface deformation under the fully developed cavitation conditions (70 psi for 30 seconds), which is attributed to the mechanical impact of HC treatment. The mean cavity area rises to 0.382±0.214 μm^2, which makes significant structural disruption. Further deformation is observed in the third column (Figure 18c, g), where the extended treatment duration (60 seconds) at the same pressure amplifies both cavity number and area. The mean cavity area reaches 0,918±1.10 μm^2, which showcase the pronounced effect of prolonged HC exposure on the clot morphology. The most deformation is seen at 70 psi for 90 seconds with 1.497±1.104 μm^2. These results collectively demonstrate a direct correlation between treatment time and clot deformation at constant pressure in the presence of HC. Notably, despite the longer exposure time of 120 seconds at 10 psi, the control group has only a minimal deformation. Furthermore, in assessing the differences between group means, a one-way analysis of variance (ANOVA) was conducted. The ANOVA test yields a P value of 0.0020, which is well below the conventional alpha level of 0.05, indicates that there are statistically significant differences among the group means (Figure 19.)

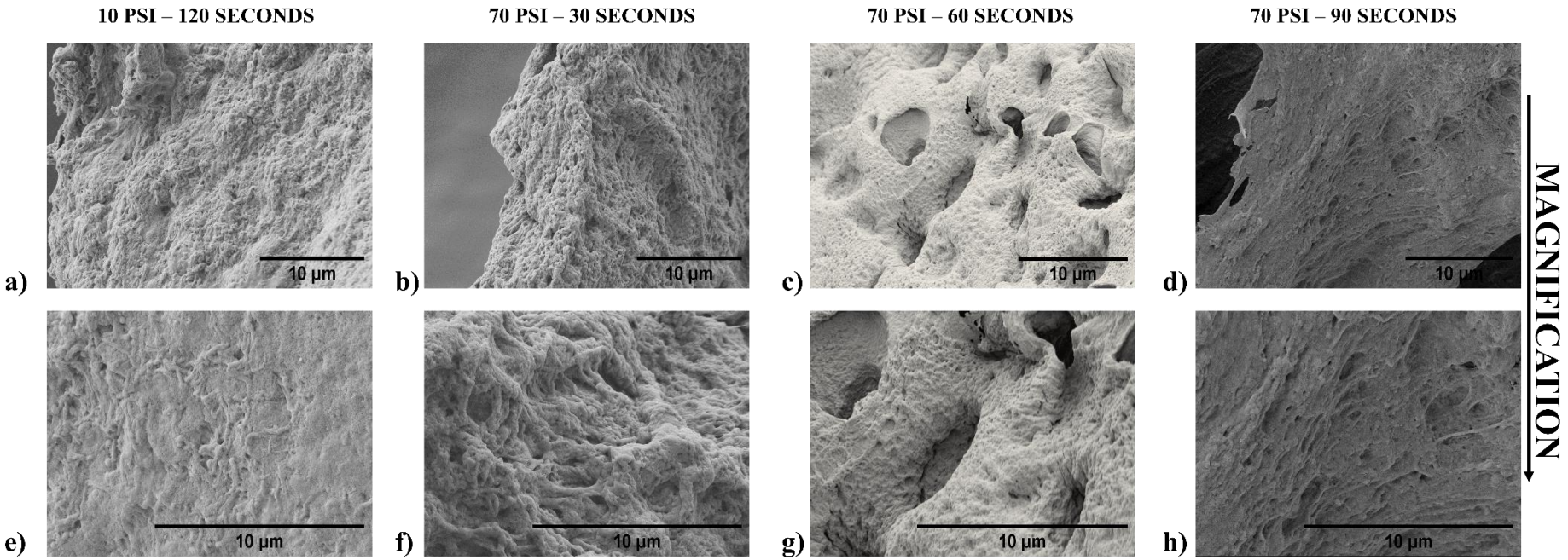

Figure 18. SEM images of surface blood clots. **a, e)** HC treatment at 10 psi (no cavitation) with 10 X, 20 X. **b, f)** HC treatment at 70 psi (fully developed cavitation) for 30 s with 10 X, 20 X. **c, g)** HC treatment at 70 psi (fully developed cavitation) for 60 s with 10 X, 20 X. **d, h)** HC treatment at 70 psi (fully developed cavitation) for 90 s with 10 X, 20 X. magnification from first row to third row, respectively.

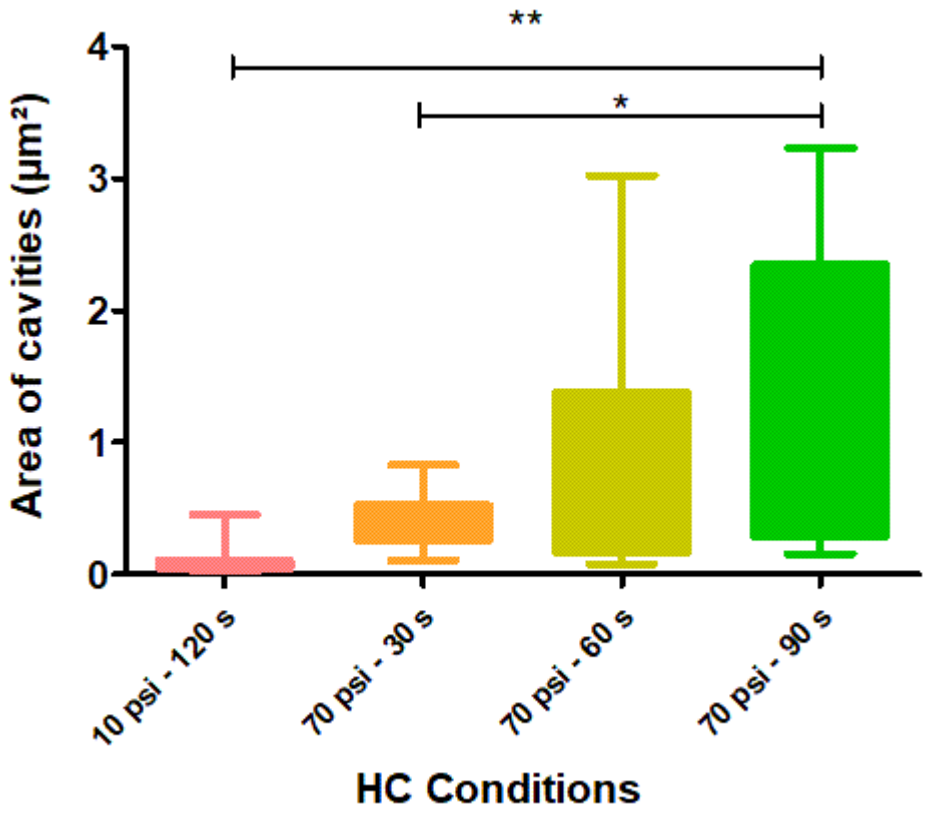

Figure 19. Area of cavities formed on the surface of blood clots upon to HC exposure of control group at 10 psi, no HC, for 120 s; at 70 psi, fully developed cavitation, for 30 s; at 70 psi, fully developed cavitation, for 60 s; at 70 psi, fully developed cavitation for 90 s.

4. DISCUSSION

This study introduces hydrodynamic cavitation induced thrombolysis using a futuristic clot-on-chip platform. The motivation of this work stems from the substantial global burden of thrombus-related diseases, notably venous thromboembolism (VTE), which stands as the third most prevalent vascular disease globally, following acute myocardial infarction and stroke (Di Nisio et al., 2016). VTE, encompassing pulmonary embolism (PE) and deep vein thrombosis (DVT), poses a considerable health challenge, with PE being a leading cause of VTE-related fatalities. Furthermore, PE, responsible for 4-5 deaths per 1000 individuals worldwide, highlight the critical need for advanced therapeutic interventions (Barco et al., 2021). Current treatments, both conventional and alternative, exhibit limitations such as heightened risks of major bleeding (Carroll et al., 2023), which necessitates regular monitoring (Le Gal & Mottier, 2012), and an increased likelihood of hemodynamic instability (Bergamo, 2014). Moreover, cautious patient selection (Neely et al., 2015) and the propensity for heating and injury to healthy tissues are further challenges regarding therapeutic modalities (Frenkel et al., 2006). The proposed CoC platform, represents a promising avenue to address these limitations, and offers a non-invasive, drug-free, and potentially more efficient solution for the treatment of thrombus-related disorders.

Considering the pressing global burden of venous thromboembolism and the limitations inherent in existing treatment options, the development of novel and effective approaches becomes paramount. This study presents compelling proof-of-concept for a potentially

transformative alternative treatment technique by HC at the micro scale.

Our findings demonstrate the CoC platform's ability to achieve both partial erosion and complete removal of blood clots. The extent of clot disruption and removal depends on directly applied pressure and exposure time (cavitation intensity). Notably, cavitation inception and fully developed cavitation are observed at relatively low upstream pressures, 10 psi and 70 psi, respectively (Figure 10-11). The cavitation inception bubbles directional flow towards the clot region, guided by the architecture of the microfluidic device, which effectively facilitates clot erosion at this pressure level. Increasing the inlet pressure to 70 psi intensifies the cavitation phenomenon, leading to the development of larger, stable cavitation clouds. Schematic of the mechanism of clot removal for those two cases will be helpful. This transition to fully developed cavitation significantly enhances clot disruption. This study provides enhanced energy efficiency and potentially reduced risk of collateral tissue damage compared to previous microfluidic HC applications where these thresholds of inception and fully developed cavitation were significantly higher (e.g., 144 psi and 1419 psi for kidney stone treatment) (Yavuz Perk et al., 2012). This favorable pressure profile underscores the CoC platform's potential in safe and efficacious translation into clinical settings.

Furthermore, our results show the CoC platform's efficacy in achieving complete clot erosion within a 2 minutes at 70 psi (Figure 14e). This is in contrast to traditional acoustic cavitation methods, which often require significantly longer exposure times (e.g., 60 minutes) and still fall short of complete clot removal (Petit et al., 2012), (Petit et al., 2015). For instance, it was reported that the weight of the blood clot was decreased from 120 mg to 50 mg after 40 minutes of acoustic cavitation treatment, which translates to an erosion rate of 1.75 mg/min (Kim et al., 2017). In comparison, our platform achieves a significantly faster erosion rate of 3.15 mg/min, which highlightes its superior efficiency and energy saving.

Moreover, the CoC platform utilizes the mechanical destructive force of cavitation to achieve clot removal, thereby eliminating the need for thrombolytic drugs. This drug-free

approach minimizes the risk of hemorrhagic events, a major concern associated with conventional thrombolytic therapies (Kasahara et al., 2011). This feature further strengthens the CoC platform's potential as a safe and efficacious alternative for VTE treatment. The observed changes in mass, diameter, and morphology of blood clots treated caused by the CoC platform demonstrate a correlation among pressure, exposure time, and underlying biophysical mechanisms. Increasing both pressure and exposure time results in more mass loss and diameter reduction, suggesting a dose-dependent relationship with clot erosion. Notably, the SEM analysis reveals an interplay between cavitation intensity and fibrin fiber integrity. At the lowest pressure (10 psi), where cavitation was absent, minimal changes can be observed, emphasizing the major role of HC. As the pressure reaches the cavitation inception point (25 psi), structural alterations begin to appear, evidenced by loosening of fibrin fibers and increasing cavity areas. Finally, at fully developed cavitation (70 psi), prolonged exposure (120 seconds) yields the most detectable changes, including significant mass and diameter reduction alongwith extensive fibrinolysis. Moreover, SEM micrographs provide evidence for the micro scale efficacy of the CoC platform in thrombolysis. The micrographs demonstrate deformation on all three key components of the blood clot: fibrin fibers, red blood cells, and platelets. This deformation disrupts the integrity of blood clot in micro scale, contributing to the observed thrombolytic effect. Platelets, which densify the fibrin network and contribute to clot stability (Kim et al., n.d.); (Kovalenko et al., 2021) are shown to be deformed after HC treatment. Similarly, red blood cells, which influence fibrin growth and clot resistance to fibrinolysis (Kovalenko et al., 2021), have deformation that compromises their functional contribution to the clot. Finally, the fibrin fibers themselves, the structural backbone of the clot (Collet et al., 2005); (Macrae et al., 2018), are fractured and fragmented, which further weakens the overall integrity of the clot. These SEM observations provide a clear visual confirmation of the HC exposure and lends strong support to the proposed mechanism of thrombolysis by the CoC platform. The platform's ability to induce these microscale deformations on all key clot components validates the proposed novel and effective thrombolysis approach.

5. Conclusion and Future Directions

This study investigated a novel "Clot-on-Chip (CoC)" platform for microscale hydrodynamic cavitation-induced thrombolysis. The platform comprised two key components: the microfluidic device and the PDMS microchip. The microfluidic device was designed and fabricated to facilitate the formation of HC bubbles at low upstream pressures. Optimized channel dimensions and surface properties enabled HC generation at low upstream pressure, which maximizes its potential for clot disruption. On the other hand, the PDMS microchip served as a chamber for precise blood clot placement. Its integration ensured optimal exposure of the clot to HC-induced forces, which enhanced the platform's efficiency and reproducibility.

This study revealed the effects of cavitation inception and fully developed cavitation on the removal of blood clots. As expected, the blood clots were eroded more during fully developed cavitation compared to cavitation inception. At constant pressure, the erosion rate also increased with time. Beyond the purely physical effects of cavitation bubbles, this study explored their impact at the biological level of blood clots. Scanning electron microscopy revealed the details of this process, which showcase the progressive damage inflicted on the clot structure of blood clots in micro scale. These results reveal the mechanical impact of cavitation treatment on clot surfaces.

The findings here present a compelling case for microscale HC as a promising, non-invasive, and drug-free approach for the use in future research effort blood clot disruption. The investigation of the intricate relationship between the cavitation effect and clot breakdown should be assessed and this innovative therapeutic technique should be optimized. Modelling efforts related to this application is necessary and should be validated against experimental data in future studies. This study opens new lanes for continued research, aiming to overcome current limitations and translate this promising

technology into effective clinical applications, potentially revolutionizing the treatment of these debilitating conditions.

New findings related to micro scale hydrodynamic cavitation suggest that the CoC may offer a strong alternative to ultrasound cavitation for fragmenting harmful entities such as blood clots. The promising results of this study lay the groundwork for future research directions in thrombolysis.

BIBLIOGRAPHY

Aghdam, A. S., Ghorbani, M., Deprem, G., Çakmak Cebeci, F., & Koşar, A. (n.d.). *A new Method for intense cavitation Bubble Generation on Layer-by-Layer Assembled SLipS*. https://doi.org/10.1038/s41598-019-48175-4

Ahmed, I., Majeed, A., & Powell, R. (2007). Heparin induced thrombocytopenia: diagnosis and management update. *Postgrad Med J*, *83*, 575–582. https://doi.org/10.1136/pgmj.2007.059188

Bagot, C. N., & Arya, R. (2008). Virchow and his triad: a question of attribution. *British Journal of Haematology*, *143*(2), 180–190. https://doi.org/10.1111/J.1365-2141.2008.07323.X

Barco, S., Valerio, L., Gallo, A., Turatti, G., Mahmoudpour, S. H., Ageno, W., Castellucci, L. A., Cesarman-Maus, G., Ddungu, H., De Paula, E. V., Dumantepe, M., Goldhaber, S. Z., Guillermo Esposito, M. C., Klok, F. A., Kucher, N., McLintock, C., Ní Áinle, F., Simioni, P., Spirk, D., … Konstantinides, S. V. (2021). Global reporting of pulmonary embolism-related deaths in the World Health Organization mortality database: Vital registration data from 123 countries. *Research and Practice in Thrombosis and Haemostasis*, *5*(5). https://doi.org/10.1002/RTH2.12520

Bartlett, J. W., De Stavola, B. L., & Meade, T. W. (2009). Assessing the contribution of fibrinogen in predicting risk of death in men with peripheral arterial disease. *Journal of Thrombosis and Haemostasis*, *7*(2), 270–276. https://doi.org/10.1111/J.1538-7836.2008.03236.X

Bates, S. M., & Weitz, J. I. (2005). New anticoagulants: Beyond heparin, low-molecular-weight heparin and warfarin. *British Journal of Pharmacology*, *144*(8), 1017–1028. https://doi.org/10.1038/SJ.BJP.0706153

Bergamo, C. (2014). Thrombolysis for pulmonary embolism and risk of all-cause mortality, major bleeding, and intracranial hemorrhage: A meta-analysis: Chatterjee S, Chakraborty A, Weinberg A, et al. JAMA 2014;311(23):2414-21. *Journal of Emergency Medicine*, *47*(5), 618. https://doi.org/10.1016/j.jemermed.2014.09.024

Bridge, K. I., Philippou, H., & Ariëns, R. A. S. (2014). Clot properties and cardiovascular disease. *Thrombosis and Haemostasis*, *112*(5), 901–908. https://doi.org/10.1160/TH14-02-0184/ID/JR0184-2/BIB

Carroll, B. J., Larnard, E. A., Pinto, D. S., Giri, J., & Secemsky, E. A. (2023). Percutaneous Management of High-Risk Pulmonary Embolism. *Circulation.*

Cardiovascular Interventions, *16*(2), E012166. https://doi.org/10.1161/CIRCINTERVENTIONS.122.012166

Collet, J. P., Shuman, H., Ledger, R. E., Lee, S., & Weisel, J. W. (2005). The elasticity of an individual fibrin fiber in a clot. *Proceedings of the National Academy of Sciences of the United States of America*, *102*(26), 9133–9137. https://doi.org/10.1073/PNAS.0504120102/ASSET/9E468249-A7CF-4A55-9EC6-5F0A08F7B161/ASSETS/GRAPHIC/ZPQ0270587210004.JPEG

Di Nisio, M., van Es, N., & Büller, H. R. (2016). Deep vein thrombosis and pulmonary embolism. *Lancet (London, England)*, *388*(10063), 3060–3073. https://doi.org/10.1016/S0140-6736(16)30514-1

Dixon, A. J., Marschner, J., Rickel, R., Shin, B. D., Klibanov, A. L., & Hossack, J. A. (1965). *In Vitro Sonothrombolysis Enhancement by Transiently Stable Microbubbles Produced by a Flow-Focusing Microfluidic Device*. https://doi.org/10.1007/s10439-017-1965-7

Engelberger, R. P., Moschovitis, A., Fahrni, J., Willenberg, T., Baumann, F., Diehm, N., Do, D.-D., Baumgartner, I., & Kucher, N. (n.d.). *Fixed low-dose ultrasound-assisted catheter-directed thrombolysis for intermediate and high-risk pulmonary embolism*. https://doi.org/10.1093/eurheartj/eht531

Fleck, D., Albadawi, H., Shamoun, F., Knuttinen, G., Naidu, S., & Oklu, R. (2017). Catheter-directed thrombolysis of deep vein thrombosis: literature review and practice considerations. *Cardiovascular Diagnosis and Therapy*, *7*(Suppl 3), S228–S237. https://doi.org/10.21037/CDT.2017.09.15

Francis, C. W., Blinc, A., Lee, S., & Cox, C. (1995). Ultrasound accelerates transport of recombinant tissue plasminogen activator into clots. *Ultrasound in Medicine and Biology*, *21*(3), 419–424. https://doi.org/10.1016/0301-5629(94)00119-X

Frenkel, V., Oberoi, J., Stone, M. J., Park, M., Deng, C., Wood, B. J., Neeman, Z., Horne, M., & Li, K. C. P. (2006). Pulsed high-intensity focused ultrasound enhances thrombolysis in an in vitro model. *Radiology*, *239*(1), 86–93. https://doi.org/10.1148/RADIOL.2391042181

Gac, S. Le, Zwaan, E., Berg, A. Van Den, & Ohl, C. D. (2007). Sonoporation of suspension cells with a single cavitation bubble in a microfluidic confinement. *Lab on a Chip*, *7*(12), 1666–1672. https://doi.org/10.1039/B712897P

Ghorbani, M., Aghdam, A. S., Gevari, M. T., Koşar, A., Cebeci, F. Ç., Grishenkov, D., & Svagan, A. J. (2020a). Facile hydrodynamic cavitation ON CHIP via cellulose

nanofibers stabilized perfluorodroplets inside layer-by-layer assembled SLIPS surfaces. *Chemical Engineering Journal*, *382*, 122809. https://doi.org/10.1016/J.CEJ.2019.122809

Ghorbani, M., Aghdam, A. S., Gevari, M. T., Koşar, A., Cebeci, F. Ç., Grishenkov, D., & Svagan, A. J. (2020b). Facile hydrodynamic cavitation ON CHIP via cellulose nanofibers stabilized perfluorodroplets inside layer-by-layer assembled SLIPS surfaces. *Chemical Engineering Journal*, *382*, 122809. https://doi.org/10.1016/J.CEJ.2019.122809

Ghorbani, M., Chen, H., Villanueva, L. G., Grishenkov, D., & Koşar, A. (2018). Intensifying cavitating flows in microfluidic devices with poly(vinyl alcohol) (PVA) microbubbles. *Physics of Fluids*, *30*(10). https://doi.org/10.1063/1.5051606/988762

Goel, L., & Jiang, X. (n.d.). *Advances in Sonothrombolysis Techniques Using Piezoelectric Transducers*. https://doi.org/10.3390/s20051288

Gogate, P. R. (n.d.). *Hydrodynamic Cavitation for Food and Water Processing*. https://doi.org/10.1007/s11947-010-0418-1

Goldhaber, S. Z., Magnuson, E. A., Chinnakondepalli, K. M., Cohen, D. J., & Vedantham, S. (2021). Catheter-directed thrombolysis for deep vein thrombosis: 2021 update. *Vascular Medicine (United Kingdom)*, *26*(6), 662–669. https://doi.org/10.1177/1358863X211042930

Gravanis, I., & Tsirka, S. E. (n.d.). *tPA as a therapeutic target in stroke*. https://doi.org/10.1517/14728222.12.2.159

Guo, S., Guo, X., Wang, X., Zhou, D., Du, X., Han, M., Zong, Y., & Wan, M. (2019). Reduced clot debris size in sonothrombolysis assisted with phase-change nanodroplets. *Ultrasonics Sonochemistry*, *54*, 183–191. https://doi.org/10.1016/J.ULTSONCH.2019.02.001

Harter, K., Levine, M., & Henderson, S. O. (2015). Anticoagulation Drug Therapy: A Review. *Western Journal of Emergency Medicine*, *XVI*(1). https://doi.org/10.5811/westjem.2014.12.22933

Itah, Z., Oral, O., Perk, O. Y., Sesen, M., Demir, E., Erbil, S., Dogan-Ekici, A. I., Ekici, S., Kosar, A., & Gozuacik, D. (2013). Hydrodynamic cavitation kills prostate cells and ablates benign prostatic hyperplasia tissue. *Experimental Biology and Medicine (Maywood, N.J.)*, *238*(11), 1242–1250. https://doi.org/10.1177/1535370213503273

Jilani, T. N., & Siddiqui, A. H. (2023). Tissue Plasminogen Activator. *StatPearls*. https://www.ncbi.nlm.nih.gov/books/NBK507917/

Kasahara, Y., Nakagomi, T., Matsuyama, T., Stern, D., & Taguchi, A. (2011). *Cilostazol Reduces the Risk of Hemorrhagic Infarction After Administration of Tissue-Type Plasminogen Activator in a Murine Stroke Model*. https://doi.org/10.1161/STROKEAHA.111.635417

Kim, J., Lindsey, B. D., Chang, W.-Y., Dai, X., Stavas, J. M., Dayton, P. A., & Jiang, X. (n.d.). *Intravascular forward-looking ultrasound transducers for microbubble-mediated sonothrombolysis*. https://doi.org/10.1038/s41598-017-03492-4

Kovalenko, T. A., Giraud, M. N., Eckly, A., Ribba, A. S., Proamer, F., Fraboulet, S., Podoplelova, N. A., Valentin, J., Panteleev, M. A., Gonelle-Gispert, C., Cook, S., Lafanechère, L., Sveshnikova, A. N., & Sadoul, K. (2021). Asymmetrical Forces Dictate the Distribution and Morphology of Platelets in Blood Clots. *Cells*, *10*(3), 1–17. https://doi.org/10.3390/CELLS10030584

Le Gal, G., & Mottier, D. (2012). *New Anticoagulants in the Treatment of VTE*. https://doi.org/10.1055/s-0032-1311799

Lippi, G., Lippi, G., Franchini, M., & Targher, G. (2011). Arterial thrombus formation in cardiovascular disease. *Nature Publishing Group*, *502*, 502–512. https://doi.org/10.1038/nrcardio.2011.91

Liu, S., Feng, X., Jin, R., & Li, G. (2018). Tissue plasminogen activator-based nanothrombolysis for ischemic stroke. *Expert Opinion on Drug Delivery*, *15*(2), 173–184. https://doi.org/10.1080/17425247.2018.1384464

López, J. A., Kearon, C., Lee, A. Y. Y., & Conde, I. D. (2004). Deep Venous Thrombosis I. PATHOPHYSIOLOGY OF DEEP VENOUS THROMBOSIS. *Hematology*. http://ashpublications.org/hematology/article-pdf/2004/1/439/1634427/439_456ash.pdf

Lu, Y., Wang, J., Huang, R., Chen, G., Zhong, L., Shen, S., Zhang, C., Li, X., Cao, S., Liao, W., Liao, Y., & Bin, J. (2016). Microbubble-Mediated Sonothrombolysis Improves Outcome After Thrombotic Microembolism-Induced Acute Ischemic Stroke. *Stroke*, *47*(5), 1344–1353. https://doi.org/10.1161/STROKEAHA.115.012056

Macrae, F. L., Duval, C., Papareddy, P., Baker, S. R., Yuldasheva, N., Kearney, K. J., McPherson, H. R., Asquith, N., Konings, J., Casini, A., Degen, J. L., Connell, S. D., Philippou, H., Wolberg, A. S., Herwald, H., & Ariëns, R. A. S. (2018). A fibrin biofilm covers blood clots and protects from microbial invasion. *The Journal of Clinical Investigation*, *128*(8), 3356–3368. https://doi.org/10.1172/JCI98734

Maegerlein, C., Friedrich, B., Berndt, M., Lucia, K. E., Schirmer, L., Poppert, H., Zimmer, C., Pelisek, J., Boeckh-Behrens, T., & Kaesmacher, J. (2018). Impact of histological thrombus composition on preinterventional thrombus migration in patients with acute occlusions of the middle cerebral artery. *Interventional Neuroradiology : Journal of Peritherapeutic Neuroradiology, Surgical Procedures and Related Neurosciences*, *24*(1), 70–75. https://doi.org/10.1177/1591019917733733

Martin, C., Sobolewski, K., Bridgeman, P., & Boutsikaris, D. (2016). *Systemic Thrombolysis for Pulmonary Embolism: A Review*. *41*(12).

Mishra, C., & Peles, Y. (2005). *Cavitation in flow through a micro-orifice inside a silicon microchannel*. https://doi.org/10.1063/1.1827602

Namli, I., Sarraf, S. S., Aghdam, A. S., Torabfam, G. C., Kutlu, O., Cetinel, S., Ghorbani, M., & Koş, A. (2022). Hydrodynamic Cavitation on a Chip: A Tool to Detect Circulating Tumor Cells. *Cite This: ACS Appl. Mater. Interfaces*, *14*, 40688–40697. https://doi.org/10.1021/acsami.2c12356

Neely, R. C., Byrne, J. G., Gosev, I., Cohn, L. H., Javed, Q., Rawn, J. D., Goldhaber, S. Z., Piazza, G., Aranki, S. F., Shekar, P. S., & Leacche, M. (2015). Surgical Embolectomy for Acute Massive and Submassive Pulmonary Embolism in a Series of 115 Patients. *The Annals of Thoracic Surgery*, *100*(4), 1245–1252. https://doi.org/10.1016/J.ATHORACSUR.2015.03.111

Nutescu, E. A., Burnett, A., Fanikos, • John, Spinler, S., & Wittkowsky, A. (n.d.). *Pharmacology of anticoagulants used in the treatment of venous thromboembolism*. https://doi.org/10.1007/s11239-015-1314-3

Opneja, A., Kapoor #1, S., & Stavrou, E. X. (n.d.). *Contribution of Platelets, the Coagulation and Fibrinolytic Systems to Cutaneous Wound Healing*. https://doi.org/10.1016/j.thromres.2019.05.001

Owens Johnson, C., Nguyen, M., Roth, G. A., Nichols, E., Alam, T., Abate, D., Abd-Allah, F., Abdelalim, A., Niguse Abraha, H., Abu-Rmeileh, N. M., Adebayo, O. M., Moshood Adeoye, A., Agarwal, G., Agrawal, S., Nidhal Aichour, A., Aichour, I., Taki Eddine Aichour, M., Alahdab, F., Ali, R., … Collaborators, S. (2019). Global, regional, and national burden of stroke, 1990â€“2016: a systematic analysis for the Global Burden of Disease Study 2016. *The Lancet Neurology*, *18*, 439–458. https://doi.org/10.1016/S1474-4422(19)30034-1

Panda, D., Saharan, V. K., & Manickam, S. (n.d.). *processes Controlled Hydrodynamic*

Cavitation: A Review of Recent Advances and Perspectives for Greener Processing. https://doi.org/10.3390/pr8020220

Pastori, D., Cormaci, V. M., Marucci, S., Franchino, G., Del Sole, F., Capozza, A., Fallarino, A., Corso, C., Valeriani, E., Menichelli, D., & Pignatelli, P. (2023). A Comprehensive Review of Risk Factors for Venous Thromboembolism: From Epidemiology to Pathophysiology. *International Journal of Molecular Sciences*, *24*(4). https://doi.org/10.3390/IJMS24043169

Patel, S. R., Hartwig, J. H., & Italiano, J. E. (2005). Review series The biogenesis of platelets from megakaryocyte proplatelets. *The Journal of Clinical Investigation*, *115*. https://doi.org/10.1172/JCI26891

Pechik, I., || Y., Mosesson, M. W., Gilliland, G. L., & || L. M. (2006). STRUCTURAL BASIS FOR SEQUENTIAL CLEAVAGE OF FIBRINOPEPTIDES UPON FIBRIN ASSEMBLY †, ‡. *Biochemistry*, *45*(11), 3588–3597. https://doi.org/10.1021/bi0525369

Periayah, M. H., Halim, A. S., Zaharil, A., & Saad, M. (2017). Mechanism Action of Platelets and Crucial Blood Coagulation Pathways in Hemostasis. *International Journal of Hematology-Oncology and Stem Cell Research IJHOSCR*, *11*(4).

Petit, B., Gaud, E., Colevret, D., Arditi, M., Yan, F., Tranquart, F., & Allémann, E. (2012). In vitro sonothrombolysis of human blood clots with BR38 microbubbles. *Ultrasound in Medicine & Biology*, *38*(7), 1222–1233. https://doi.org/10.1016/J.ULTRASMEDBIO.2012.02.023

Petit, B., Yan, F., Bussat, P., Bohren, Y., Gaud, E., Fontana, P., Tranquart, F., & Allémann, E. (2015). Fibrin degradation during sonothrombolysis – Effect of ultrasound, microbubbles and tissue plasminogen activator. *Journal of Drug Delivery Science and Technology*, *25*(February), 29–35. https://doi.org/10.1016/J.JDDST.2014.12.001

Qiu, S., Zhong, S., Feng, Q., Wang, Y., Li, D., Zhan, J., Lyu, C., Deng, Z., Zha, D., & Wu, J. (2022). Sono-assisted-thrombolysis by three-dimensional diagnostic ultrasound improves epicardial recanalization and microvascular perfusion in acute myocardial infarction. *Quant Imaging Med Surg*, *12*(10). https://doi.org/10.21037/qims-21-1247

Ramjan Ali, M., Salim Hossain, M., Ariful Islam, M., Saiful Islam Arman, M., Sarwar Raju, G., Dasgupta, P., & Fariha Noshin, T. (2014). *Aspect of Thrombolytic Therapy: A Review*. https://doi.org/10.1155/2014/586510

Randolph, S. A. (2016). Ischemic Stroke. *Workplace Health and Safety*, *64*(9), 444. https://doi.org/10.1177/2165079916665400

Ribas, J., Valcárcel, J., Alba, E., Ruíz, Y., Cuartero, D., Iriarte, A., María Mora-Luján, J., Huguet, M., Cerdà, P., Martínez-Yélamos, S., Corbella, X., Santos, S., & Riera-Mestre, A. (2021). Clinical Medicine Catheter-Directed Therapies in Patients with Pulmonary Embolism: Predictive Factors of In-Hospital Mortality and Long-Term Follow-Up. *J. Clin. Med*, *10*, 4716. https://doi.org/10.3390/jcm10204716

Scarabin, P. Y., Arveiler, D., Amouyel, P., Dos Santos, C., Evans, A., Luc, G., Ferrières, J., & Juhan-Vague, I. (2003). Plasma fibrinogen explains much of the difference in risk of coronary heart disease between France and Northern Ireland. The PRIME study. *Atherosclerosis*, *166*(1), 103–109. https://doi.org/10.1016/S0021-9150(02)00309-X

Seminar. (n.d.). https://doi.org/10.1016/S0140-6736(16)30514-1

Seyedmirzaei Sarraf, S., Rokhsar Talabazar, F., Namli, I., Maleki, M., Sheibani Aghdam, A., Gharib, G., Grishenkov, D., Ghorbani, M., & Koşar, A. (2022). Fundamentals, biomedical applications and future potential of micro-scale cavitation-a review. *Lab on a Chip*, *22*(12), 2237–2258. https://doi.org/10.1039/D2LC00169A

Suo, D., Guo, S., Lin, W., Jiang, X., & Jing, Y. (2015). Thrombolysis using multi-frequency high intensity focused ultrasound at MHz range: an in vitro study. *Physics in Medicine & Biology*, *60*(18), 7403. https://doi.org/10.1088/0031-9155/60/18/7403

Tanne, D., Benderly, M., Goldbourt, U., Boyko, V., Brunner, D., Graff, E., Reicher-Reiss, H., Shotan, A., Mandelzweig, L., & Behar, S. (2001). A prospective study of plasma fibrinogen levels and the risk of stroke among participants in the bezafibrate infarction prevention study. *American Journal of Medicine*, *111*(6), 457–463. https://doi.org/10.1016/S0002-9343(01)00914-7

Umerah, C. o., & Momodu, I. I. (2023). Anticoagulation. *Cardiology Board Review, Second Edition*, 615–626. https://doi.org/10.1002/9781119814979.ch30

Unnithan, A. K. A., Das, J. M., & Mehta, P. (2023). Hemorrhagic Stroke. *StatPearls*. https://www.ncbi.nlm.nih.gov/books/NBK559173/

Vassalli, J.-D., Sappino, A.-P., & Bein, D. (n.d.). *Perspectives The Plasminogen Activator/Plasmin System*.

Versteeg, H. H., Heemskerk, J. W. M., Levi, M., & Reitsma, P. H. (2013). NEW FUNDAMENTALS IN HEMOSTASIS. *Physiol Rev*, *93*, 327–358.

https://doi.org/10.1152/physrev.00016.2011

Weisel, J. W., & Litvinov, R. I. (n.d.). *Fibrin Formation, Structure and Properties*. https://doi.org/10.1007/978-3-319-49674-0_13

Wu, T.-H., Chen, Y., Park, S.-Y., Hong, J., Teslaa, T., Zhong, J. F., Carlo, D. Di, Teitell, M. A., & Chiou, P.-Y. (2012). *Pulsed laser triggered high speed microfluidic fluorescence activated cell sorter †, ‡*. https://doi.org/10.1039/c2lc21084

Yamamoto, T. (2018). Management of patients with high-risk pulmonary embolism: A narrative review. *Journal of Intensive Care*, *6*(1), 1–9. https://doi.org/10.1186/S40560-018-0286-8/FIGURES/3

Yau, J. W., Teoh, H., & Verma, S. (2015a). Endothelial cell control of thrombosis. *BMC Cardiovascular Disorders*, *15*(1), 1–11. https://doi.org/10.1186/S12872-015-0124-Z/TABLES/2

Yau, J. W., Teoh, H., & Verma, S. (2015b). *Endothelial cell control of thrombosis*. https://doi.org/10.1186/s12872-015-0124-z

Yavuz Perk, O. (2012). *MICROSCALE HYDRODYNAMIC CAVITATION AND ITS BIOMEDICAL APPLICATIONS*.

Yavuz Perk, O., Gozuacik, D., & Kos, A. (n.d.). *Kidney Stone Erosion by Micro Scale Hydrodynamic Cavitation and Consequent Kidney Stone Treatment*. https://doi.org/10.1007/s10439-012-0559-7

Yeh, C. H., Gross, P. L., & Weitz, J. I. (2014). Evolving use of new oral anticoagulants for treatment of venous thromboembolism. *Blood*, *124*(7), 1020. https://doi.org/10.1182/BLOOD-2014-03-563056

Zhang, K., Jiang, Y., Zeng, H., & Zhu, H. (2023). Application and risk prediction of thrombolytic therapy in cardio-cerebrovascular diseases: a review. *Thrombosis Journal*, *21*(1), 1–16. https://doi.org/10.1186/S12959-023-00532-0/TABLES/2